Journal of Computational Physics 335 (2017) 179–200

Contents lists available at ScienceDirect

Journal of Computational Physics

www.elsevier.com/locate/jcp

Goal-based h-adaptivity of the 1-D diamond difference discrete ordinate method

R.S. Jeffers [a,b,*], J. Kópházi [a], M.D. Eaton [a], F. Févotte [b], F. Hülsemann [b], J. Ragusa [c]

[a] Department of Mechanical Engineering, Imperial College of Science, Technology and Medicine, Prince Consort Road, London, SW7 2AZ, UK
[b] EDF R&D, EDF Lab Paris-Saclay, 7 Boulevard Gaspard Monge, 91120 Palaiseau, France
[c] Texas A&M University, Department of Nuclear Engineering, College Station, TX 77843, USA

ARTICLE INFO

Article history:
Received 20 July 2016
Received in revised form 14 November 2016
Accepted 18 January 2017
Available online 25 January 2017

Keywords:
Goal-based
Error estimation
Diamond difference
Neutron transport
DWR
AMR

ABSTRACT

The quantity of interest (QoI) associated with a solution of a partial differential equation (PDE) is not, in general, the solution itself, but a functional of the solution. Dual weighted residual (DWR) error estimators are one way of providing an estimate of the error in the QoI resulting from the discretisation of the PDE.

This paper aims to provide an estimate of the error in the QoI due to the spatial discretisation, where the discretisation scheme being used is the diamond difference (DD) method in space and discrete ordinate (S_N) method in angle. The QoI are reaction rates in detectors and the value of the eigenvalue (K_{eff}) for 1-D fixed source and eigenvalue (K_{eff} criticality) neutron transport problems respectively. Local values of the DWR over individual cells are used as error indicators for goal-based mesh refinement, which aims to give an optimal mesh for a given QoI.

1. Introduction

Goal-based dual weighted residual (DWR) methods have already been applied to the field of neutron transport for solvers that discretise in space using the finite element method, a method for which the development of DWR error estimates is very mature. Despite the increased use of finite element codes in the industry, many full scale production codes use the diamond difference (DD) method for solving the discrete ordinate (S_N) angular discretisation of the neutron transport equation. Examples include the PARTISN code developed at LANL [1], the Denovo S_N module in the SCALE code (developed at ORNL) [2] and the DOMINO solver that is a part of EDF's COCAGNE code [3]. Reliable error estimates are desirable to ensure that the error in a calculated quantity of interest (QoI) due to spatial discretisation is within a prescribed tolerance. The derivation and application of rigorously derived goal-based DWR error estimators has not yet been applied to the diamond difference method.

In addition to this, full core pressurised water reactor (PWR) eigenvalue (K_{eff}) problems often require the solution of a large number of degrees of freedom (number of unknowns) due to the discretisation of a seven dimensional phase space. $\mathcal{O}(10^{12})$ DoF were used recently in the DOMINO solver [3]. Being able to reduce this number by only refining the spatial mesh where needed, for a specific QoI, would also be useful in producing computationally efficient solutions. Using

* Corresponding author.
E-mail address: rebecca.s.jeffers@gmail.com (R.S. Jeffers).

http://dx.doi.org/10.1016/j.jcp.2017.01.037

goal-based DWR error indicators to guide adaptive mesh refinement (AMR) would be essential in this case since it has been shown that AMR using error indicators that aim to reduce the global error in the forward solution can, in certain circumstances, fail to yield an accurate answer to the QoI compared to uniform refinement (see [4, p. 783], [5, p. 306], [6, p. 3]).

The focus of this paper is the development, implementation and application of goal-based DWR error estimates and AMR to the 1-D DD spatial discretisation of the S_N discretised neutron transport equation. This is a necessary step before extending these methods to multidimensional problems. The estimators are derived for fixed source and eigenvalue (K_{eff} criticality) problems and the QoI can be linear or non-linear (detector response and the value of K_{eff} respectively).

Many researchers in reactor physics have implemented goal-based error estimation and mesh refinement techniques to finite element (FE) approximations of the neutron transport equations. Wang and Ragusa in particular have investigated goal-based error estimators and indicators for the spatial error in the diffusion approximation [7], simplified P_N (SP_N) equations (along with Turcksin and Bangerth) [5] and the S_N approximation of the neutron transport equation [4], where the spatial dimension was discretised using either continuous (for diffusion and SP_N) or discontinuous (for S_N transport) FEs.

Lathouwers applied the DWR goal-based scheme described in a text book by Bangerth and Rannacher [8] to drive h-adaptation in the discontinuous FE spatial discretisation of the discrete ordinate (S_N) angularly discretised transport equation (DG-FEM-S_N). Both detector functions [9] and eigenvalues [10] were investigated as QoI. The difference between Lathouwers's work and Wang and Ragusa's work for S_N transport is that Lathouwers calculates the DWR for each angle and integrates via quadrature, whereas Wang and Ragusa take the norm of the difference between the approximate solution and a reference solution (the solution obtained on a refined/higher order mesh) of either the scalar flux or current, then weight this by the norm of the same error estimate for the adjoint solution [4].

Goffin et al. [11] also applied a DWR h-adaptive mesh refinement scheme to the transport equations with the eigenvalue being the QoI. In this case the angular discretisation used was the spherical harmonics (P_N) discretisation with a sub-grid scale finite element spatial discretisation. This work was later extended to provide both regular and goal-based angular adaptivity, by allowing the order of the spherical harmonic (P_N) expansion to be different at each node of the mesh for each energy group [12].

An error indicator for spatial refinement of the Arbitrarily High Order Transport Method of the Nodal type (AHOT-N) was derived by Duo et al. [13], with the aim of reducing the global L^2 error norm. Although duality arguments are used in the derivation of the error estimator, a dual solution is not required for its evaluation, since the error in the adjoint solution is replaced by bounds to that term in terms of the forward solution. Similar arguments were used by Park et al. for spatial and angular adaptivity of the of the FE-P_N discretisation of the even parity equations [14]. It is noted that, in both of these cases, the goal quantity is limited to be the L^2 error, hence the mesh which results may not be optimal for other quantities of interest.

Researchers outside of the neutronics field have investigated how to apply goal-based error estimators to methods other than FEs [15]. Giles and Pierce lay out the theory for general discretisation schemes noting that the function given by a FE solution could be used, or a function could be fit through nodal values of other discretisation schemes [16,17]. Chen et al. take a similar approach to presenting a general functional analytic framework for the DWR (goal-based) *a posteriori* error estimation for general discretisation methods, but handle the hyperbolic case more rigorously [18].

Venditti and Darmofal obtain a discrete adjoint equation from the discretised forward equations rather than discretising the continuous adjoint equations [19]. Kuzmin et al. also employed the technique of obtaining a DWR method from an arbitrary numerical scheme by deriving a finite element interpolant of the resulting values [20,21]. Some attempts have been made to reformulate difference schemes as variational problems so that a variation on the DWR scheme used in FE can be employed. Collins et al. applied this idea to the Lax–Wendroff finite difference scheme [22].

This paper extends the work of Chen et al. [18] to the system of coupled S_N equations that are then discretised by the DD method. Chen et al. mention that finite volume (FV) schemes do not require the adjoint solution to be approximated in a space that is larger than the forward solution since FV schemes "do not naturally fit into variational forms" [18, p. 70]. We show that in the 1D-DD scheme, Galerkin orthogonality applies to the test functions, which are in a different space than the approximate forward solution. It is for this reason that Galerkin orthogonality does not apply to the adjoint solution calculated on the same mesh as the forward equation (see section 4.4). We also show that, for the DD scheme, the discretised adjoint equations must be derived from the continuous adjoint equations, not obtained by transposing the discretised forward equations as in the work of Venditti et al. [19].

All goal-based DWR schemes require the solution of both a forward and an adjoint equation. When error estimation is coupled with mesh refinement, the computational overhead of calculating the adjoint solution is often more than made up for by the saving made by the reduction in the number of DoF in the system. In all Bubnov–Galerkin FE cases the adjoint solution must be calculated on a mesh that is more refined than the forward equation due to Galerkin orthogonality [8–10]. Some variants of the goal-based method involve calculating the solution on two separate meshes for both the forward and adjoint equations [4]. This paper shows that for the DD equations, only one forward and one adjoint solution is required, and that in almost all cases analysed here, calculating an adjoint solution on the same mesh as the forward is sufficient to give a good error indicator for refinement. In most cases, the accuracy of the overall error estimation is also sufficient in this case.

A more accurate solution to the adjoint equation does, however, provide a more accurate estimation to the error in the QoI (see section 4.4). For this reason, the code is equiped with the higher-order DD method derived for the 1-D equations by Hennart [23] and the comparison of the accuracy of the error estimation obtained with adjoint solutions of different accuracy is investigated.

This paper is organised as follows. Section 2 derives the discrete ordinates equations. Section 3 shows how the traditional and Hennart-type higher order DD-S_N schemes in 1-D are weighted residual (WR) schemes. Section 4 combines the ideas presented by Rannacher et al. for non-linear DWR error estimated problems [8,24] to the ideas expressed in Chen and Gunzburger's work to derive a DWR error estimator for DD-S_N discretisation of the fixed source and eigenvalue (K_{eff}) neutron transport problems, for both linear and non-linear QoI. Sections 5 and 6 explain the implementation of these DWR (goal-based) adaptivity algorithms as well as an assessment of the accuracy of the error estimation and computational efficiency of the adaptive method (in terms of number of cells required for a given solution accuracy). A variety of fixed source and eigenvalue (K_{eff}) neutron transport verification test cases are solved. Finally, we conclude by providing an overall assessment of the performance and accuracy of the DWR adaptive algorithms and indicate potential extensions to the work in section 7.

2. Angular discretisation of the 1-D mono-energetic neutron transport equation

The one-group continuous neutron transport equation, assuming isotropic scattering, is given by equation (1):

$$\mu\frac{\partial\psi(x,\mu)}{\partial x}+\Sigma_t(x)\psi(x,\mu)=\frac{\Sigma_{s0}(x)}{2}\phi(x)+q(x,\mu)\quad\text{for }-1\le\mu\le+1\text{ and }0\le x\le\ell. \tag{1}$$

x is the spatial coordinate, μ is the angular cosine of the flux direction, $\Sigma_t(x)$ is the total macroscopic cross-section (cm^{-1}) and Σ_{s0} is the isotropic scattering macroscopic cross-section (cm^{-1}). $\psi(x,\mu)$ is the angular flux ($cm^{-2}s^{-1}sr^{-1}MeV^{-1}$) integrated over the azimuthal angle, and assumed constant with respect to time and energy. $q(x,\mu)$ is the angular fixed source ($cm^{-3}s^{-1}sr^{-1}MeV^{-1}$) integrated over the azimuthal angle, assumed constant with respect to time and energy. The scalar flux is given by:

$$\phi(x)=\int_{-1}^{+1}\psi(x,\mu)d\mu \tag{2}$$

and has the units: ($cm^{-2}s^{-1}MeV^{-1}$). The discrete ordinate (S_N) approximation discretises the angular domain along discrete ordinates as follows:

$$\mu_j\frac{d\psi_j(x)}{dx}+\Sigma_t(x)\psi_j(x)=\frac{\Sigma_{s0}(x)}{2}\phi(x)+q_j(x)\quad,\quad\text{for }j=1,2,\ldots,m\text{ and }0\le x\le\ell, \tag{3}$$

where everything is defined as in equation (1) but that the subscript j indicates a quantity along the jth quadrature point, m is the number of ordinates in the angular discretisation and the scalar flux is now approximated by numerical integration (quadrature):

$$\phi(x)\approx\sum_{j=1}^{m}w_j\psi_j(x). \tag{4}$$

w_j are the weights associated with ordinates taken at quadrature points j in the domain $-1\le\mu\le1$. In this work the quadrature points and weights are given by Gauss–Legendre quadrature.

3. The diamond difference discrete ordinate (DD-S_N) equations as a weighted residual (WR) scheme

One can view the diamond difference scheme in 1-D as a weighted residual (WR) scheme that seeks an approximation to the strong solution of the angularly discretised neutron transport equation. We shall explain how in this section. We start by looking at the situation for a single ordinate, fixed source, pure absorption problem with a Dirichlet boundary condition in section 3.1. This is extended to multi-angle problems that include scattering operators in section 3.2, and criticality problems in section 3.3 where the ordinates are also coupled by the fission operator. The view of the DD scheme as a WR scheme is also described in Pitkäranta using a single ordinate, purely absorbing, fixed source problem [25].

3.1. Single-ordinate problem

In this section, the notation $\psi(x)$ represents an angular flux along a particular direction. The single ordinate, fixed source, pure absorption problem is then written as:

$$\mu \frac{d\psi(x)}{dx} + \Sigma_t(x)\psi(x) = q(x), \tag{5}$$

$$\psi(0) = \psi_D, \tag{6}$$

assuming $\mu > 0$ and where ψ_D is a fixed incoming flux. Note that the j subscript is omitted in this section because we are considering a single ordinate only.

The WR method is a general mathematical approach to solving partial differential equations (PDEs) that encompasses many different types of numerical discretisation schemes. The point collocation, sub-domain, Bubnov–Galerkin (traditional method for FE codes) and Petrov–Galerkin methods all satisfy the definition of a WR method. This is because they involve weighting the residual of the PDE by a series of test functions, integrating over the solution domain and setting the resulting integral to zero.

In our case, the data and source terms exist in L^2. Thus, the differential term must also exist in L^2 for equation (5) to be satisfied in an integral sense:

$$\int_0^\ell R(x)v(x)dx = 0, \quad \forall v \in L^2, \tag{7}$$

where ℓ is the length of the spatial domain, and the $R(x)$ is the residual:

$$R(x) = q(x) - \mu \frac{d\psi(x)}{dx} - \Sigma_t(x)\psi(x). \tag{8}$$

A *strong* solution is sought in H^1 (as opposed to a classical solution in C^1 [26]) to the integral equation (7) that also satisfies the boundary condition (6). Due to the residual being in L^2 the resulting integral equation must hold if weighted by any function in L^2.

In the DD scheme an approximate solution, $\psi_h(x)$, is sought in an n dimensional subspace of H^1: $\psi_h(x) \in U^h \subset H^1$. $\psi_h(x)$ can be expanded in terms of a set of independent basis functions of U^h: the set of trial functions, $N_i(x)$:

$$\psi_h(x) = \sum_{i=1}^{n} c_i N_i(x). \tag{9}$$

In the traditional DD method, there is one trial function, N_i, associated with each node, i, in the spatial domain. Higher order DD approximations also include cell-centred trial functions.

In Hennart's formulation [23], the flux within cell i is expanded in terms of a set of basis functions as follows:

$$\psi_{h,p,i}(x) = \psi_i N_i(x) + \psi_{i+1} N_{i+1}(x) + \sum_{k=0}^{p-2} \psi_{c,i}^k N_{c,i}^k(x) \quad \text{for } x_i \le x \le x_{i+1}, \tag{10}$$

where h indicates that the solution is approximate and p denotes the order of approximation in the cell. $p = 1$ for the traditional low order DD scheme. ψ_i is the flux value at node i, and $\psi_{c,i}^k$ is the k'th cell central moment of the flux in cell i.

We define:

$$\zeta = \frac{2x - x_i - x_{i+1}}{\Delta x_i}. \tag{11}$$

The basis functions are then defined, depending on the order p inside a cell, in terms of normalised Legendre polynomials as follows [23]:

$$N_i(x) = \frac{1}{2}(-1)^{p-1}\left[P_{p-1}(\zeta) - P_p(\zeta)\right] \tag{12}$$

$$N_{i+1}(x) = \frac{1}{2}\left[P_{p-1}(\zeta) + P_p(\zeta)\right] \tag{13}$$

$$N_{c,i}^k(x) = P_k(\zeta) + P_{p-2+m(k)}(\zeta), \quad \text{for } k = 0, \ldots p-2; \tag{14}$$

$m(k) = 1$ or 2 such that $k - 2 + m(k)$ has the same parity as k. $P_k(\zeta)$ is the normalised Legendre polynomial of degree k over the reference cell $[-1, +1]$. We also note that these basis functions map out a subspace of H^1 for any p. The Legendre polynomials have all the properties specified in equation 1.5 of Hennart's paper [23], these are repeated below:

$$P_k(+1) = 1, \tag{15}$$

$$P_k(-1) = (-1)^k, \tag{16}$$

$$\int_{-1}^{+1} P_k(\zeta) P_l(\zeta) d\zeta = \delta_{kl} N_k, \tag{17}$$

$$\int_{x_i}^{x_{i+1}} P_k\left(\frac{2x - x_i - x_{i+1}}{\Delta x_i}\right) P_l\left(\frac{2x - x_i - x_{i+1}}{\Delta x_i}\right) dx = \frac{\Delta x_i}{2} \int_{-1}^{+1} P_k(\zeta) P_l(\zeta) d\zeta = \delta_{kl} N_k \frac{\Delta x_i}{2}, \tag{18}$$

where $N_k = \frac{2}{2k+1}$ and δ_{kl} is the Kronecker delta.

The cell central moments of a function $u(x)$ defined over a cell i are as follows:

$$m^k_{c,i}(u(x)) = \frac{\int_{x_i}^{x_{i+1}} u(x) P_k\left(\frac{2x - x_i - x_{i+1}}{\Delta x_i}\right) dx}{\int_{x_i}^{x_{i+1}} P_k\left(\frac{2x - x_i - x_{i+1}}{\Delta x_i}\right) P_k\left(\frac{2x - x_i - x_{i+1}}{\Delta x_i}\right) dx}, \tag{19}$$

$$= \frac{\int_{-1}^{+1} u(\frac{\zeta \Delta x_i + x_i + x_{i+1}}{2}) P_k(\zeta) d\zeta}{N_k}. \tag{20}$$

The boundary conditions are essential, so we further constrict the space of allowable functions to U^h_b: the space that has a Dirichlet boundary condition at ψ_b ($\psi_b = \psi_1$ for right-going ordinates, $\psi_b = \psi_n$ for left-going ordinates). This set is $n-1$ dimensional and has $n-1$ unknowns.

To solve for the remaining coefficients in equation (9), a set of $n-1$ independent equations are obtained by weighting the residual by $n-1$ test functions. In the DD scheme, these are obtained from a subset of L^2 (a different subset from the set of trial functions), and are discontinuous over cell boundaries. We therefore have a Petrov–Galerkin scheme, where the trial and test functions are not the same, and as the dimension of the subspaces tend to infinity, we obtain a strong solution to the transport equation (7). The advantage of a strong solution is that the resulting approximation, $\psi_h(x)$, is regular enough to apply the operators of the equation to them, thus we can easily calculate the residual that results from $\psi_h(x)$, then weight it by the adjoint solution to obtain a DWR error estimator (see section 4).

The set of locally defined test functions for a p-ordered cell, defined over the interval $[x_i, x_{i+1}]$ is therefore:

$$M_{i,k}(x) = \begin{cases} P_k\left(\frac{2x - x_i - x_{i+1}}{\Delta x_i}\right) & \text{if } x \in [x_i, x_{i+1}] \\ 0 & \text{otherwise} \end{cases} \quad \text{for} \quad k = 1, 2, \ldots p-1 \text{ and } i = 1, 2, \ldots, nc, \tag{21}$$

where nc is the total number of cells in the domain.

The cell equations for cell number i can then be written as:

$$\frac{2\mu}{N_k \Delta x_i} \left\{ \left[\psi_{i+1} - (-1)^k \psi_i \right] - \int_{-1}^{+1} \psi_h(\zeta) \frac{dP_k(\zeta)}{d\zeta} d\zeta \right\} + \Sigma_{t,i} \psi^k_c = m^k_c(q), \quad k = 0, \ldots p-1. \tag{22}$$

The formula for the elements of the inverse of the $p \times p$ matrix, given by equation (22), is hard-coded into the code for a given cell order p.

3.2. Multi-angle problems

To extend this method to multi-angle problems, we must consider the solution, $\Psi \in \left(H^1\right)^m := \bar{U}$. Each element of the m-sized vector represents a flux solution for a particular ordinate direction μ_j that exists in H^1. As previously mentioned in section 2, the values of μ_j are determined by Gauss–Legendre quadrature of order m. Ordinates μ_1 to $\mu_{\frac{m}{2}}$ represent the positive ordinates in increasing magnitude and ordinates $\mu_{\frac{m}{2}+1}$ to μ_m represent the negative ordinates in decreasing magnitude.

The continuous-in-space and discretised-in-angle equation we aim to approximate, (3), can therefore be represented as follows (in the fixed source case):

$$W \mathcal{A} \Psi = W Q. \tag{23}$$

$\Psi \in \bar{U}$ with the i'th element corresponding to the continuous function representing the angular flux in direction i. $Q \in \left(L^2\right)^m := \bar{V}$ is the discretised in angle fixed source vector. Each element i corresponds to the fixed source in direction i, which is a function in the L^2 space. $\mathcal{A}$ is an $m \times m$ matrix, the diagonal contains the streaming and absorption operators for each angle and the off-diagonals contain isotropic scattering terms multiplied by the corresponding angular weight, as shown for the general case below:

$$\mathcal{A} = \begin{bmatrix} \mu_1 \frac{d}{dx} - \Sigma_t - \frac{\Sigma_s w_1}{2} & \cdots & -\frac{\Sigma_s w_j}{2} & \cdots & -\frac{\Sigma_s w_m}{2} \\ \frac{\Sigma_s w_1}{2} & \cdots & \mu_j \frac{d}{dx} - \Sigma_t - \frac{\Sigma_s w_j}{2} & \cdots & -\frac{\Sigma_s w_m}{2} \\ \frac{\Sigma_s w_1}{2} & \cdots & -\frac{\Sigma_s w_j}{2} & \cdots & \mu_m \frac{d}{dx} - \Sigma_t - \frac{\Sigma_s w_m}{2} \end{bmatrix}. \tag{24}$$

$\mathcal{A}$ represents a mapping $\bar{U} \to \bar{V}$. W is a diagonal matrix consisting of the angular weights. Because its inverse exists, we know that solving $\mathcal{A}\Psi = Q$, is equivalent to solving equation (23). It is used here to represent the importance of the individual angular equations relative to one another. The following notation is adopted:

$$\mathcal{K} = W\mathcal{A}. \tag{25}$$

The S_N problem, before spatial discretisation, is a matrix equation to solve for Ψ. Boundary conditions are applied to Ψ by imposing that the solution exists in a subset of the space $\bar{U}$, denoted by $\bar{U}_b$. $\bar{U}_b$ is the set of all functions in $\bar{U}$ that satisfy the particular boundary conditions. In the forward equation, boundary conditions are imposed on the incoming boundaries. Thus for ordinates with $\mu_j > 0$, a Dirichlet boundary condition is applied to the left-most node and a Dirichlet boundary condition is applied to the right-most node for ordinates with $\mu_j < 0$. For simplicity of explanation we shall assume vacuum boundary conditions, hence we replace $\bar{U}_b$ by $\bar{U}_{0_i}$, where 0 represents a vacuum boundary condition and i represents the fact that this is imposed on incoming boundaries. It is clear that $\bar{U}_{0_i} \subset \bar{V}$, it is also dense in $\bar{V}$. Due to all the terms in equation (23) existing in $\bar{V}$, the integral statement of the equation can be denoted by taking the scalar product defined in this space with a test function in this space. An appropriate scalar product defined for the space $\bar{V}$ would be:

$$\langle a, b \rangle_{\bar{V}} = \int a^T b dx \quad \forall a, b \in \bar{V}. \tag{26}$$

Hence the integral statement form of the equation is defined as:

Find $\Psi \in \bar{U}_{0_i}$ such that:

$$\langle \mathcal{K}\Psi, v \rangle_{\bar{V}} = \langle W Q, v \rangle_{\bar{V}} \quad \forall v \in \bar{V}. \tag{27}$$

This equation can be solved approximately using the DD equations. This is achieved by taking the solution to be in a finite dimensional subset: $\bar{U}^h_{0_i} \subset \bar{U}_{0_i}$. In the DD equation $\bar{U}^h_{0_i}$ is defined by the space of all m sized vectors, where elements 1 to $\frac{m}{2}$ are functions in $U^h_{0_L} \subset H^1_{0_L}$ (where the subscript 0_L denotes that the left boundary of the spatial domain is a vacuum boundary condition), and elements $\frac{m}{2} + 1$ to m are functions in $U^h_{0_R} \subset H^1_{0_R}$ (where the subscript 0_R denotes that the right boundary of the spatial domain is a vacuum boundary condition). This space is mapped out in each ordinate by n independent basis functions ($n \times m$ basis functions in total). The unknown coefficients are solved by m boundary conditions (one for each ordinate) and $(n-1) \times m$ weighting functions. These weighting functions are taken from a subspace of $\bar{V}$ denoted by $\bar{V}_h \subset \bar{V}$, mapped out in each ordinate by $n-1$ basis functions ($(n-1) \times m$ basis functions in total).

3.3. Eigenvalue problems

The same method can be applied to the eigenvalue equation. In this case we want to solve the equation:

$$\mu_j \frac{d\psi_j}{dx} + \Sigma_t \psi_j - \frac{\Sigma_{s0}}{2}\phi - \frac{\nu\Sigma_f}{2K_{eff}}\phi = 0 \quad \text{for } j = 1, 2, \ldots, m \quad , \tag{28}$$

with the following normalisation condition:

$$\sum_{j=1}^{m} w_j \int_0^{\ell} \frac{\nu\Sigma_f}{2}\phi\psi_j dx = \int_0^{\ell} \frac{\nu\Sigma_f}{2}\phi\phi dx = 1. \tag{29}$$

Σ_f is a spatially varying fission cross-section and ν is the averaged number of neutrons released per fission. Equations (28) and (29) can be expressed as a matrix equation in angle, and a differential equation in space as follows:

Find $\Psi \in \bar{U}_{0_i}$ and $\lambda \in \mathbb{R}$ such that:

$$\mathcal{K}\Psi = \lambda W \mathcal{F}\Psi, \tag{30}$$

$$\langle W\mathcal{F}\Psi, \Psi \rangle_{\bar{V}} = 1. \tag{31}$$

Everything is defined as before. $\lambda = \frac{1}{K_{eff}}$. $\mathcal{F}$ is an $m \times m$ matrix, each element contains the function that represents the spatial variation of the fission cross section (in this case single group): $\frac{\nu\Sigma_f}{2}$ multiplied by an angular weight w_i, where i represents the column number as follows:

$$\mathcal{F} = \begin{bmatrix} \frac{\nu\Sigma_f w_1}{2} & \dots & \frac{\nu\Sigma_f w_j}{2} & \dots & \frac{\nu\Sigma_f w_m}{2} \\ \frac{\nu\Sigma_f w_1}{2} & \dots & \frac{\nu\Sigma_f w_j}{2} & \dots & \frac{\nu\Sigma_f w_m}{2} \\ \frac{\nu\Sigma_f w_1}{2} & \dots & \frac{\nu\Sigma_f w_j}{2} & \dots & \frac{\nu\Sigma_f w_m}{2} \end{bmatrix} \tag{32}$$

The operator $\mathcal{F}$ represents a mapping: $\bar{V} \to \bar{V}$. Note that equation (30) is equivalent to equation (28) but with each ordinate equation multiplied by its corresponding weighting function.

We can express both the eigenvalue equation and the normalisation condition as WR statements. This can be arrived at by expressing the residual of equation (30) as:

$$R = \lambda W \mathcal{F}\Psi - \mathcal{K}\Psi, \tag{33}$$

then multiplying this by a test function $v \in \bar{V}$ and integrating over the phase space and setting the result to zero. This is equivalent to writing:

$$\langle R, v\rangle_{\bar{V}} = 0 \quad \forall v \in \bar{V}. \tag{34}$$

The normalisation condition can be multiplied by a test scalar:

$$\tau r = \tau\left[\langle W\mathcal{F}\Psi, \Psi\rangle_{\bar{V}} - 1\right] = 0 \quad \forall \tau \in \mathbb{R}. \tag{35}$$

Both of these combined result in the WR statement for the eigenvalue problem:

$$\langle R, v\rangle_{\bar{V}} + \tau r = 0. \tag{36}$$

The aim is to find both a function, Ψ, and a scalar, λ, that satisfies the WR statement (36). This problem can be viewed as finding a member:

$$\hat{\Psi} = \{\Psi, \lambda\} \in \hat{\bar{U}}_{0_i} \tag{37}$$

where

$$\hat{\bar{U}}_{0_i} := \bar{U}_{0_i} \times \mathbb{R} \tag{38}$$

such as in [10]. The test function space is then defined as:

$$\hat{v} = \{v, \tau\} \in \hat{\bar{V}} \text{ where } \hat{\bar{V}} := \bar{V} \times \mathbb{R}. \tag{39}$$

The WR statement of equation (36) can be expressed using similar notation to [10]:

Find $\hat{\Psi} \in \hat{\bar{U}}_{0_i}$ such that:

$$A(\hat{\Psi}; \hat{v}) = \lambda F(\Psi, v) - B(\Psi, v) + \tau(F(\Psi, \Psi) - 1) = 0 \quad \forall \hat{v} \in \hat{\bar{V}} \quad , \tag{40}$$

where $A(\cdot;\cdot)$ is a semi-linear form: non-linear in the argument that precedes the semi-colon and linear in the argument that follows the semi-colon. The operators in equation (40) are defined in terms of the inner product over $\bar{V}$ as follows:

$$F(\cdot,\cdot) = \langle W\mathcal{F}\cdot, \cdot\rangle_{\bar{V}} \quad : \quad \bar{V} \times \bar{V} \to \mathbb{R}, \tag{41}$$

$$B(\cdot,\cdot) = \langle \mathcal{K}\cdot, \cdot\rangle_{\bar{V}} \quad : \quad \bar{U} \times \bar{V} \to \mathbb{R}. \tag{42}$$

In our case we are taking the weighting functions from a different space to the trial functions since we are going to discretise using the DD approximation, this is not the case for the equivalent expression given in [10].

In the DD approximation, the solution $\hat{\Psi}_h$ is taken from a space $\hat{\bar{U}}^h_{0_i} \subset \hat{\bar{U}}_{0_i}$. The $m \times n$ coefficients for the basis functions of the approximate solution space are solved for by m boundary conditions, and $m \times (n-1)$ basis functions of the space $\hat{\bar{V}}_h \subset \hat{\bar{V}}$.

4. Expressing the error in a goal functional as a DWR

In this section the DWR scheme for the DD-S_N fixed source and eigenvalue equations are explained. We seek an estimation of the numerical error in a goal quantity due to the spatial discretisation. In the fixed source case the goal quantity is a detector function (a linear QoI) and in the eigenvalue case, it is the eigenvalue itself (a non-linear QoI). It is highlighted here that the detector function is defined throughout the whole domain and hence it can be non-zero in multiple regions in order to represent reaction rates required in multiple positions in the reactor.

The work in this section combines the original ideas expressed by Ranncher et al. [8,24], that were applied specifically to the DGFEM-S_N neutron transport method by Lathouwers [9,10], with the generalisation to non-Galerkin discretisation schemes given by Giles, Pierce and Chen [16–18]. Section 4.1 shows the general scheme for any linear or semi-linear form. In both cases the form is obtained by weighting an equation for which the solution is in a space U, by a function in a space V, of which U is a dense subspace. The main distinction from Rannacher's work is that $U \neq V$ in our case. The specific application to fixed source and eigenvalue problems in neutron transport is explained in sections 4.2 and 4.3 respectively.

4.1. General Petrov–Galerkin case

We consider the general semi-linear form on a vector space V:

$$A(\cdot;\cdot) : U \times V \to \mathbb{R} \text{ where } U \text{ is dense in } V, \tag{43}$$

which is non-linear with respect to any parameter before the semi-colon and linear with respect to anything after it.

There is a problem to be solved for $u \in U$ defined by the WR equation (44):

$$A(u; v) = 0 \quad \forall v \in V, \tag{44}$$

where U is dense in V.

There exists a QoI defined by a functional (linear or non-linear) of the solution to equation (44) which we shall denote by:

$$J(u) : U \to \mathbb{R}. \tag{45}$$

Becker and Rannacher derive an approach to estimating the error in the functional: $J(u) - J(u_G)$ where u_G is the solution to a Bubnov–Galerkin approximation to equation (44) by using "the framework of optimal control" [24, p. 5 and p. 9]. A similar method is followed here to obtain an estimate for the numerical error due to spatial discretisation when the approximate solution is solved using a DD-S_N discretisation method.

One can look at the problem of finding $J(u)$ from the solution $u \in U$ of the problem described in equation (44) as a trivial equality constrained optimisation problem [24]:

$$\text{Minimise } J(u), \text{ given the constraint that: } A(u; v) = 0 \quad \forall v \in V \text{ and } u \in U. \tag{46}$$

It is trivial because the value of $J(u)$ is unique provided that u is the solution of the equality constraint equation. We therefore use the method of Lagrangian multipliers where we define a Lagrange multiplier z, and obtain the Lagrangian [27]:

$$L(u, z) = J(u) + A(u; z) \text{ given the constraint that } u \in U \text{ and } z \in V. \tag{47}$$

If $J(\psi)$ is a minimum of $J(u)$ for the original constrained problem, there exists $\psi^\dagger$ such that $L(\psi, \psi^\dagger)$ is a stationary point of the Lagrangian [27].

A stationary point is where the Gateaux partial derivatives of $L(u, z)$ with respect to both parameters u and z are zero in all directions. We denote this idea by the following notation for the Gateaux partial derivatives of the Lagrangian:

$$L'_u(u, z)[y] \quad \text{and} \quad L'_z(u, z)[y]. \tag{48}$$

The quantity in square brackets denotes the direction in which the Gateaux derivative is taken (in this case, direction y). The $'$ denotes a first order derivative and the corresponding subscript denotes with respect to which parameter the derivative is being taken.

To find the stationary point of $L(u, z)$, denoted by $L(\psi, \psi^\dagger)$, we must satisfy the following equations:

$$L'_u(\psi, \psi^\dagger)[y] = J'_u(\psi)[y] - A'_u(\psi; \psi^\dagger)[y] = 0 \quad \forall y \in U, \tag{49}$$

$$L'_z(\psi, \psi^\dagger)[g] = J'_z(\psi)[g] - A'_z(\psi; \psi^\dagger)[g] = 0 \quad \forall g \in V. \tag{50}$$

We note that equation (50) can be simplified to:

$$L'_z(\psi, \psi^\dagger)[g] = -A'_z(\psi; \psi^\dagger)[g] = 0 \quad \forall g \in V. \tag{51}$$

This equation is satisfied if ψ is the solution to the forward equation, no matter what the definition of $\psi^\dagger \in V$. $\psi^\dagger$ in this equation can be replaced by any $z \in V$ and the equality will still hold. We know from the forward problem that $A(\psi; v)$ is a constant value of zero for all functions $v \in V$. Hence the gradient with respect to the second parameter is zero for all functions $v \in V$. Therefore this component of the derivative cannot be used to determine the value of $\psi^\dagger$.

Thus, the adjoint problem reduces to finding a value $\psi^\dagger$ that satisfies the equation:

$$L'_u(\psi, \psi^\dagger)[y] = J'_u(\psi)[y] - A'_u(\psi; \psi^\dagger)[y] = 0 \quad \forall y \in U. \tag{52}$$

The means of finding the value $\psi^\dagger$ will depend on the particular problem (two examples are treated in the following sections).

We can use equation (52) to give a value for $J(\psi) - J(\psi_h)$, where ψ_h is an approximation of ψ in the U space (for example, the lowest order DD approximation). We do this by considering the case where y in equation (52) is equal to $e = \psi - \psi_h \in U$:

$$J'_u(\psi)[\psi - \psi_h] - A'_u(\psi; \psi^\dagger)[\psi - \psi_h] = 0, \tag{53}$$

which can be expressed as:

$$J(\psi) - J(\psi_{\mathrm{h}}) = A(\psi; \psi^{\dagger}) - A(\psi_{\mathrm{h}}; \psi^{\dagger}) + \epsilon, \tag{54}$$

where:

$$\epsilon = \sum_{l=1}^{t-1} \frac{\left\{ J_u^l(\psi)[\psi - \psi_{\mathrm{h}}] - A_u^l(\psi; \psi^{\dagger})[\psi - \psi_{\mathrm{h}}] \right\}}{l!} (\psi - \psi_{\mathrm{h}})^l + \mathcal{O}(\psi - \psi_{\mathrm{h}})^t. \tag{55}$$

However, the first term of ϵ is zero from the optimisation problem, and $A(\psi; \psi^{\dagger}) = 0$ by definition of the WR problem. Therefore we have an estimate for the error given by an adjoint WR and a linearisation error ϵ:

$$J(\psi) - J(\psi_{\mathrm{h}}) = -A(\psi_{\mathrm{h}}; \psi^{\dagger}) + \epsilon, \tag{56}$$

where:

$$\epsilon = \frac{\left\{ J_u''(\psi)[\psi - \psi_{\mathrm{h}}] - A_u''(\psi; \psi^{\dagger})[\psi - \psi_{\mathrm{h}}] \right\}}{2!} (\psi - \psi_{\mathrm{h}})^2 + \mathcal{O}(\psi - \psi_{\mathrm{h}})^3. \tag{57}$$

Two examples are discussed in the sections that follow. Section 4.2 discusses the example where $A(u; v) = 0$ represents the fixed source neutron transport problem with $J(u)$ representing a detector function goal value. Section 4.3 discusses the example where $A(u; v) = 0$ represents a neutron transport eigenvalue ($\mathrm{K_{eff}}$ criticality) problem with $J(u)$ being the eigenvalue. We shall assume for now that any iteration error in the scatter/eigenvalue problems are negligible (see section 4.4 for further discussion). To simplify the discussion we assume vacuum boundary conditions. The subscript 0_{i} will be used to note a space where the vacuum boundary conditions are defined on the left boundary for positive ordinates and on the right boundary for negative ordinates. The opposite will be noted by the subscript 0_{o}.

4.2. Fixed source problem with detector function goal

In this case we have the following definition for the semi-linear form:

$$A(u; v) = \langle \mathcal{K}u, v \rangle_{\bar{V}} - \langle W\, Q\,, v \rangle_{\bar{V}} \text{ with } u \in \bar{U}_{0_i} \text{ and } v \in \bar{V}. \tag{58}$$

The problem to be solved is the following:

Find $\Psi \in \bar{U}_{0_{\mathrm{i}}}$ such that

$$A(\Psi; v) = \left(\langle \mathcal{K}\Psi, v \rangle_{\bar{V}} - \langle W\, Q\,, v \rangle_{\bar{V}} \right) = 0 \quad \forall v \in \bar{V}. \tag{59}$$

The goal quantity is a linear functional on $\bar{U}_{0_{\mathrm{i}}}$:

$$J(\Psi) = \langle \Psi, W \boldsymbol{\Sigma}_{\mathrm{d}} \rangle_{\bar{V}}. \tag{60}$$

Ψ is the solution to equation (59). $\boldsymbol{\Sigma}_{\mathrm{d}}$ is an m sized vector, each element j is the detector cross section distribution for angle j, denoted by: $\Sigma_{\mathrm{d}j} \in L^2$. $\boldsymbol{\Sigma}_{\mathrm{d}}$ can represent a single detector or multiple detectors throughout the reactor since it is defined over the whole spatial and angular domain.

Hence, equation (52) becomes:

$$L_u'(\Psi, \Psi^{\dagger})[y] = \frac{\partial}{\partial u} \left(\langle \Psi, W\, \Sigma_{\mathrm{d}} \rangle_{\bar{V}} + \langle W\, Q\,, \Psi^{\dagger} \rangle_{\bar{V}} - \langle \mathcal{K}\Psi, \Psi^{\dagger} \rangle_{\bar{V}} \right)[y] = 0$$
$$\forall y \in \bar{U}_{0_i}\,,\ \Psi^{\dagger} \in \bar{V} \text{ and } \Psi \text{ a solution to equation (59)}, \tag{61}$$

which reduces to:

$$\frac{\partial}{\partial u} \left(\langle \Psi, W\, \Sigma_{\mathrm{d}} \rangle_{\bar{V}} - \langle \mathcal{K}\Psi, \Psi^{\dagger} \rangle_{\bar{V}} \right)[y] = 0 \quad \forall y \in \bar{U}_{0_{\mathrm{i}}}\,,\ \Psi^{\dagger} \in \bar{V} \text{ and } \Psi \text{ a solution to equation (59)}. \tag{62}$$

$\frac{\partial}{\partial u}(\cdot)[y]$ denotes the partial Gateaux derivative with respect to parameter u (in equations (61) and (62) u is Ψ) in the direction y.

It can be shown that equation (62) holds for the solution of the following adjoint equation:

$$\langle v, W\, \Sigma_{\mathrm{d}} \rangle_{\bar{V}} - \langle v, \mathcal{K}^{\dagger}\Psi^{\dagger} \rangle_{\bar{V}} = 0 \quad \forall v \in \bar{V} \text{ and } \Psi^{\dagger} \in D(\mathcal{K}^{\dagger}) \subset \bar{V}, \tag{63}$$

where $D(\mathcal{K}^{\dagger})$ is the space of functions in the domain of the adjoint operator. Note that $D(\mathcal{K}^{\dagger}) = \bar{U}_{0_o}$ [28], and therefore $D(\mathcal{K}^{\dagger}) \neq D(\mathcal{K})$ [18].

We can now use equation (62) to obtain an expression for the error in the linear functional $J(\Psi) - J(\Psi_{\mathrm{h}})$ where Ψ_{h} is the DD approximation. This is done by taking $y = \Psi - \Psi_{\mathrm{h}}$ in equation (62) and following the same logic as in equations (53)–(57) so that one arrives at:

$$J(\Psi) - J(\Psi_h) = -A(\Psi; \Psi^\dagger) + \epsilon. \tag{64}$$

$\epsilon = 0$ due to linearity, consequently equation (64) reduces to:

$$J(\Psi) - J(\Psi_h) = \langle W Q - \mathcal{K}\Psi_h, \Psi^\dagger \rangle_{\bar{V}} \tag{65}$$

$$= \langle R_h, \Psi^\dagger \rangle_{\bar{V}} \tag{66}$$

Hence the error in the goal quantity can be obtained by weighting the residual of the DD solution with the solution to the adjoint equation defined by equation (63).

4.3. Eigenvalue problem with eigenvalue goal

In this case we recall definitions (37)–(42) and have the following definition for the semi-linear form [8,10]:

$$A(\hat{u}; \hat{v}) = \lambda F(u, v) - B(u, v) + \tau(F(u, u) - 1) \quad : \quad \hat{\bar{U}} \times \hat{\bar{V}} \to \mathbb{R}, \tag{67}$$

where $\hat{u} \in \hat{\bar{U}}$ and $\hat{v} \in \hat{\bar{V}}$.

The problem to be solved is:

Find $\hat{\Psi} \in \hat{\bar{U}}_{0_i}$ such that:

$$A(\hat{\Psi}; \hat{v}) = \lambda F(\Psi, v) - B(\Psi, v) + \tau(F(\Psi, \Psi) - 1) = 0 \quad \forall \hat{v} \in \hat{\bar{V}}. \tag{68}$$

The boundary conditions are contained in the space of allowable functions $\hat{\bar{U}}_{0_i}$.

The goal quantity is the non-linear functional on $\hat{\bar{U}}_{0_i}$ defined by [8,10]:

$$J(\hat{\Psi}) = \lambda F(\Psi, \Psi) = \lambda. \tag{69}$$

Therefore equation (52) becomes:

$$L'_{\hat{u}}(\hat{\Psi}, \hat{\Psi}^\dagger) = J'_{\hat{u}}(\hat{\Psi})[\hat{y}] - A'_{\hat{u}}(\hat{\Psi}; \hat{\Psi}^\dagger)[\hat{y}] = 0 \quad \forall \hat{y} \in \hat{\bar{U}}_{0_i}, \hat{\Psi}^\dagger \in \hat{\bar{V}} \text{ and } \hat{\Psi} \text{ being the solution to equation (68).} \tag{70}$$

Setting $\hat{y} = \{y, \xi\}$ and $\hat{\Psi}^\dagger = \{\Psi^\dagger, \lambda^\dagger\}$ this becomes:

$$\lambda\{F(\Psi, y) + F(y, \Psi)\} + \xi F(\Psi, \Psi) = \lambda F(y, \Psi^\dagger) - B(y, \Psi^\dagger) + \xi F(\Psi, \Psi^\dagger) + \lambda^\dagger\{F(\Psi, y) + F(y, \Psi)\}$$
$$\forall \hat{y} \in \hat{\bar{U}}_{0_i}, \hat{\Psi}^\dagger \in \hat{\bar{V}} \text{ and } \hat{\Psi} \text{ the solution to equation (68)}, \tag{71}$$

which rearranges to:

$$\lambda F(y, \Psi^\dagger) - B(y, \Psi^\dagger) + \xi\{F(\Psi, \Psi^\dagger) - F(\Psi, \Psi)\} + (\lambda^\dagger - \lambda)\{F(\Psi, y) + F(y, \Psi)\} = 0$$
$$\forall \hat{y} \in \hat{\bar{U}}_{0_i}, \hat{\Psi}^\dagger \in \hat{\bar{V}} \text{ and } \hat{\Psi} \text{ the solution to equation (68).} \tag{72}$$

This is the same as in Lathouwers's paper [10], but we remain in the non-discretised formulation of the WR.

We see from equation (72) that this equation is satisfied by using the value of $\hat{\Psi}^\dagger = \{\Psi^\dagger, \lambda^\dagger\}$ found by the solution to the adjoint eigenvalue equation, with the following specific normalisation condition:

Find $\Psi^\dagger \in \bar{U}$ and $\lambda^\dagger \in \mathbb{R}$ such that:

$$\mathcal{K}^\dagger \Psi^\dagger = \lambda^\dagger \mathcal{G}^\dagger \Psi^\dagger \tag{73}$$

$$\langle \mathcal{G}^\dagger \Psi^\dagger, \Psi \rangle_{\bar{V}} = 1. \tag{74}$$

Where $\mathcal{G}^\dagger$ is the adjoint of the operator $\mathcal{G} = W\mathcal{F}$. $\mathcal{G}$ is a linear bounded operator on $\bar{V}$ and so its adjoint operator is easily defined by:

$$\langle \mathcal{G}u, v \rangle_{\bar{V}} = \langle u, \mathcal{G}^\dagger v \rangle_{\bar{V}} \quad \forall v, u \in \bar{V}. \tag{75}$$

In fact, the mono energetic fission operator is self-adjoint $\mathcal{G} = \mathcal{G}^\dagger$. However, $\Psi^\dagger$ is still restricted to be part of the subspace $\bar{U}_{0_o}$, due to the $\mathcal{K}^\dagger$ operator.

We therefore know that $\langle \mathcal{G}^\dagger \Psi^\dagger, \Psi \rangle_{\bar{V}} \equiv F(\Psi, \Psi^\dagger)$ and we can express the integral statement of (73) and (74) as:

$$\lambda^\dagger \langle \mathcal{G}^\dagger \Psi^\dagger, v \rangle_{\bar{V}} - \langle \mathcal{K}^\dagger \Psi^\dagger, v \rangle_{\bar{V}} + \tau \left(\langle \mathcal{G}^\dagger \Psi^\dagger, \Psi \rangle_{\bar{V}} - 1 \right) = 0 \quad \forall \hat{v} := \{v, \tau\} \in \hat{\bar{V}}. \tag{76}$$

Bell and Glasstone show that $\lambda = \lambda^\dagger$ [29]. We note that the solution $\hat{\Psi}^\dagger$ is the same for all $\hat{v} \in \hat{\bar{V}}$. Hence the solution will remain the same if $\hat{v}$ was replaced by any $\hat{y} \in \hat{\bar{U}}_{0_i}$, since $\hat{\bar{U}}_{0_i}$ forms a dense subset of $\hat{\bar{V}}$. When taken from this subset, the $\langle \mathcal{K}^\dagger \Psi^\dagger, y \rangle_{\bar{V}}$ term can be replaced by $\langle \mathcal{K} y, \Psi^\dagger \rangle_{\bar{V}}$. With these considerations taken in to account, we see that the first 3 terms of equation (72) are equivalent to equation (76) with the weighting function being taken from a particular subspace of $\hat{\bar{V}} : \hat{\bar{U}}_{0_i}$. Then the fact that the adjoint and forward eigenvalues are the same means that the final term also goes to zero. Hence, the solution to the integral statement of the adjoint eigenvalue problem (76) gives the value $\hat{\Psi}^\dagger$ required in equation (70).

Now that the values of both $\hat{\Psi}$ and $\hat{\Psi}^\dagger$ are known, it is desirable to have equation (70) in a form such that it gives an approximation to $J(\Psi) - J(\Psi_h)$. This involves considering equation (70) for the case where $\hat{y} = e = \hat{\Psi} - \hat{\Psi}_h \in \hat{\bar{U}}_{0_i}$ and following the logic of equations (53)–(57) to arrive at the following error estimator:

$$J(\hat{\Psi}) - J(\hat{\Psi_h}) = -A(\hat{\Psi_h}, \hat{\Psi}^\dagger) + \epsilon, \tag{77}$$

where

$$\epsilon = \frac{\left\{ J''_{\hat{\Psi}}(\hat{\Psi})[\hat{\Psi} - \hat{\Psi}_h] - A''_{\hat{\Psi}}(\hat{\Psi}; \hat{\Psi^\dagger})[\hat{\Psi} - \hat{\Psi}_h] \right\}}{2!} (\hat{\Psi} - \hat{\Psi}_h)^2 + \mathcal{O}(\hat{\Psi} - \hat{\Psi}_h)^3 \tag{78}$$

and

$$\begin{aligned} A(\hat{\Psi}_h; \hat{\Psi}^\dagger) &= \lambda F(\Psi_h, \Psi^\dagger) - B(\Psi_h, \Psi^\dagger) + \lambda^\dagger (F(\Psi_h, \Psi_h) - 1) \\ &= \lambda F(\Psi_h, \Psi^\dagger) - B(\Psi_h, \Psi^\dagger), \end{aligned} \tag{79}$$

since $F(\Psi_h, \Psi_h) = 1$ is the normalisation applied in the numerical solver.

It is assumed that ϵ is small compared to the WR part since it is second order with respect to the discretisation error. However, there are cases where ϵ is not small compared to the DWR. For example, where the second order derivatives are very large. This effect should reduce upon refinement as the error in the forward solution is reduced.

4.4. Calculating the DWR in practice

In general, the analytical solution to the adjoint equation is not available, and so an approximation to $\Psi^\dagger$ must be used. In this work the forward equation is solved using the lowest order DD approximation which corresponds to a linear variation within the cell. In this case Ψ_h is generated from a Petrov–Galerkin method that uses piece-wise constant test functions. A piece-wise constant approximation to $\Psi^\dagger$ would result in an error estimate of zero due to Galerkin orthogonality. It is similar reasoning that means that the adjoint solution must be computed in a different space from the forward equation in Bubnov–Galerkin FE approaches [8–10]. In Bubnov–Galerkin approaches, either a higher-order FE needs to be used for the adjoint solution, or the number of cells in the discretisation increased (or both). In the DD case, however, if we obtain an approximate adjoint solution from a DD discretisation of the adjoint equations, using the same order and the same mesh as the forward equation, we obtain a piece-wise linear approximation to the adjoint solution, not piece-wise constant. Hence the approximate adjoint solution is not in the space of test functions and the DWR calculated using this approximation will not give zero.

One can also see from equations (63) and (76) that we cannot simply transpose the discrete operators obtained by the DD-S_N discretisation of the forward equations to give a discrete approximation of the adjoint equation (as in the work of Venditti and Darmofal [19]). This is because the discretisation would not be consistent with the strong formulation of the continuous adjoint equations. Although the weighting functions used in the DD approximation of the forward equations are members of $\bar{V}$ and are therefore consistent with the strong formulation of the forward equations (equations (27) and (40) for the fixed source and eigenvalue problems respectively), they are not members of $D(\mathcal{K}^\dagger)$. Consequently, although the DD approximation of the forward equation is consistent with the continuous forward equation, using the transpose of the resulting discretised operators to approximate the adjoint equation does not lead to a consistent discretisation of the adjoint equations. Solving the DD-S_N discretisation of the strong formulation of the adjoint solution (63) with appropriate boundary conditions gives an approximate adjoint solution in a subspace of the correct phase space, $D(\mathcal{K}^\dagger)$, and the discretised equations are consistent with the continuous equations. Implementing this is not computationally difficult for the DD scheme since the forward sweep algorithm can be used in reverse for the adjoint equations.

Chen and Gunzburger [18] note that because FV methods do not naturally fit into variational forms, the Galerkin orthogonality problem does not apply. However, in our case, we have shown that Galerkin orthogonality does apply to some functions, but not the function that results from calculating the adjoint solution on the same mesh as the forward equation.

However, as was noted by Chen and Gunzburger [18], the more accurate the approximation to the adjoint solution, the more accurate the error estimator, thus there may be benefits to obtaining a higher-order solution to the adjoint equation. In this work we test the error estimated by using an adjoint computed on the same mesh, one twice as refined, and one using a higher-order DD approximation using Hennart's method [23].

In addition to this we can note that instead of weighting the residual of the lowest order DD solution by $\Psi^\dagger$, we could have weighted the residual by $\Psi^\dagger - \bar{\Psi}^\dagger$, where $\bar{\Psi}^\dagger$ is the average value of the adjoint over the cell. Assuming zero iteration error, these two choices result in identical answers. This is because any constant component of the adjoint solution weighted with the residual will go to zero, due to Galerkin orthogonality. In reality, the component weighted by the average will give a measure of the iteration error [30,31]. In this paper we do not investigate the use of goal-based iteration error approximation for use in solver iteration exit criteria. We iterate until the residual weighted by unity is as close to machine precision as possible.

In practice, the weighted residual of equations (66) and (79) (with the adjoint solution being replaced by an appropriate approximate solution) can be calculated cell-wise by expressing the values of both R_h and $\Psi^\dagger$ for a given ordinate and cell as a sum of weighted Legendre polynomials. The integral over the cell is then easily calculated for each discrete ordinate direction. A weighted sum of the DWR for each ordinate is performed to obtain the value of the integral over a single cell. The cell values can then be used as error indicators for refinement or summed to obtain an estimation of the error.

5. Implementation

The code written for this paper is a 1-D, one-group fixed source and eigenvalue DD-S_N code. The spatial discretisation is achieved by using an arbitrary order DD formulation as described in section 3.

After the forward equations are solved on a simple mesh, local error indicators are calculated by a DWR method using one of three different approximations to the adjoint solution. The local error indicators are used to calculate a total error estimator for the QoI. If the error is above a user-defined tolerance and the user-defined maximum number of mesh iterations has not yet been reached, then the mesh is refined. In the case of AMR, any cell with local error indicator greater than $\alpha * maxerror$ is refined, where *maxerror* is the greatest local error indicator in the mesh and α is a value between 0 and 1.

Three different DWR error estimators are tested. If the forward solution is expressed as $\psi_{\mathrm{h},p}$ and the resulting residual from that expressed as $R_{\mathrm{h},p}$, where h represents the mesh on which the solution is calculated and p represents the order of accuracy at which the solution is calculated in the cells throughout the domain, then the three error estimators tested in this paper are:

$$E_1 = \sum_{i=1}^{nc} |E_{1i}| \quad \text{where} \quad E_{1i} = \sum_{j=1}^{m} w_j (R_{\mathrm{h},p,j}, \psi^\dagger_{j,\mathrm{h},p})_i, \tag{80}$$

$$E_2 = \sum_{i=1}^{nc} |E_{2i}| \quad \text{where} \quad E_{2i} = \sum_{j=1}^{m} w_j (R_{\mathrm{h},p,j}, \psi^\dagger_{j,\frac{\mathrm{h}}{2},p})_i, \tag{81}$$

$$E_3 = \sum_{i=1}^{nc} |E_{3i}| \quad \text{where} \quad E_{3i} = \sum_{j=1}^{m} w_j (R_{\mathrm{h},p,j}, \psi^\dagger_{j,\mathrm{h},p+1})_i. \tag{82}$$

$(\cdot,\cdot)_i$ is the L^2 inner product over cell i. The cell-wise values E_{1i}, E_{2i} and E_{3i} shall be referred to as local error indicators. Estimator E_1 is likely to be the least accurate due to the arguments given in section 4.4. Estimators E_2 and E_3 increase the accuracy of the error estimation by increasing the accuracy of the adjoint equation. One would expect the h-refined adjoint solution (used in E_2) to be most appropriate when the adjoint solution contains sharp gradients. The p-refined adjoint solution (used in E_3) is expected to be most appropriate in the case of sufficiently smooth adjoint solutions.

Four different test cases are used to test the theory presented in this paper. Test cases 1 to 3 are fixed source test cases and test case 4 is an eigenvalue test case. These test cases were chosen since they all have an analytical solution to the flux (and eigenvalue in test case 4). The test cases and the rationale for selecting each one are described below.

Test case 1 is a 1-D 8 cm long reactor with vacuum boundary conditions on both sides. The material properties are homogeneous with $\Sigma_t = 1.0$, $\Sigma_{s0} = 0.5$ and unit isotropic source. We used $\alpha = 0.5$ for this test case as it was found to give stable results. The analytical solution to this problem was derived by hand. Test case 1a and 1b are identical, but the former's goal quantity is the integral of the scalar flux throughout the whole domain and the latter is the integral of the scalar flux in the first 1 cm of the domain. This is a simple test case used as an initial test. It should also show the difference between the error estimate obtained for different goal values on the same test case.

Test case 2 uses the Reed cell problem geometry, described in [32]. An analytical solution to the S_8 approximation of the scalar flux is given in [33]. The analytical solution is plotted in Fig. 1. This test case was chosen for its added complexity (highly heterogeneous cross sections). It should therefore give a better idea of the behaviour of the error estimators and indicators. It is also known that the DD equations give oscillatory scalar fluxes in areas of large total cross sections and small μ [32] because of the possible presence of negative angular fluxes when the cell width is larger than $\frac{2|\mu|}{\Sigma_\mathrm{t}}$ [34]. This test case therefore provides an extreme case for testing the methods derived in this paper. The worst region in the Reed cell problem for this phenomena is where $\Sigma_\mathrm{t} = 50.0\ \mathrm{cm}^{-1}$. When S_8 is used, the smallest value of the cosine of the angle is $\mu = 0.183434642495650$. In this region Δx must be smaller than about 0.007 cm to satisfy the negative flux criterion. Because of this we test the problem on two different starting meshes.

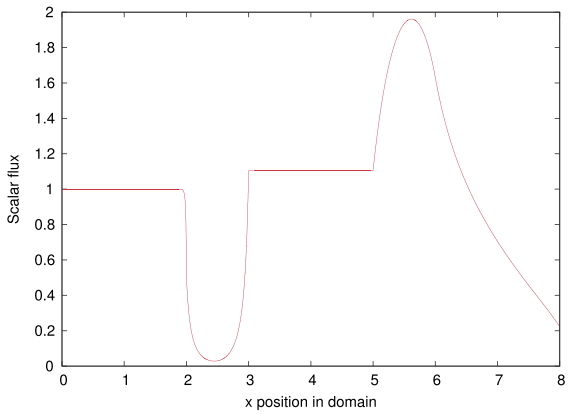

Fig. 1. Reed cell problem scalar flux solution.

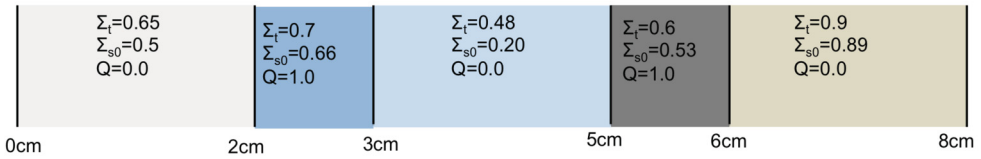

Fig. 2. EIRA-1-D problem definition.

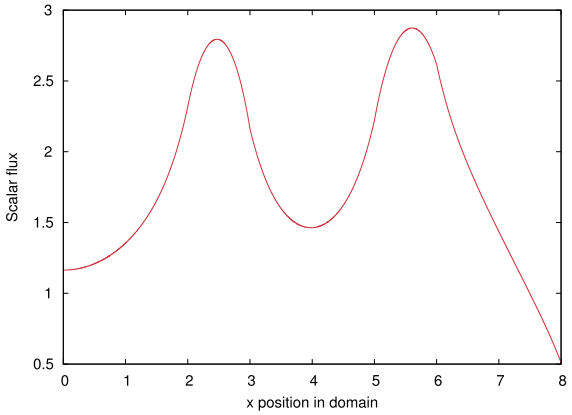

Fig. 3. EIRA-1-D problem scalar flux solution.

The difference between test cases 2a and 2b are that the QoI (goals) are different in each case. In test case 2a the goal is the integral of the scalar flux throughout the whole domain. The goal of test case 2b is the integral of the scalar flux in the first 1 cm of the domain, this was chosen to see how the method behaved when the goal was placed in the region which is especially challenging for the DD method. We used $\alpha = 0.3$ for this test case as it was found to give stable results.

Test case 3: the EIRA-1-D problem, takes the geometry of the Reed cell benchmark, but replaces the cross sections with less extreme values. The cross sections are those defined for the EIRA-2A benchmark problem defined in [35]. The geometry definition is given in Fig. 2. The differences between test cases 3a and 3b are yet again the QoI for which we want an optimal mesh. In test case 3a the QoI is the integral of the scalar flux throughout the whole domain. For test case 3b it is the integral in the first 1 cm of the domain. A refined solution to this problem is plotted in Fig. 3. We used $\alpha = 0.3$, as for the Reed cell benchmark. An analytical solution to the scalar flux was obtained by using the MAPLE code written by Warsa [33]. Test case 3 has less harsh discontinuities than test case 2 and a higher scatter ratio. Test case 3 therefore allows the methods to be tested on a heterogeneous geometry which is still a reasonable choice for the DD method.

Finally, test case 4 is an eigenvalue test case. It is a homogeneous vacuum boundary problem. The methods described by Siewert [36] were used to derive an analytical solution for the critical width of the domain, ℓ_0, for the S_2 case with vacuum boundary conditions on both sides of the slab. ℓ_0 is given as an input to the code and we then see how close the calculated K_{eff} result is to unity. Test case 4 was chosen to enable us to test the method on an eigenvalue problem for which an analytical solution is available.

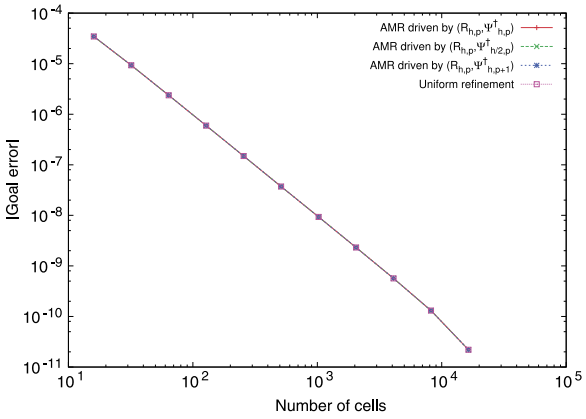

(a) The absolute value of the goal error as a function of the cell number. AMR refinement criterion: refine if local error indicator $> 0.5 * maxerror$

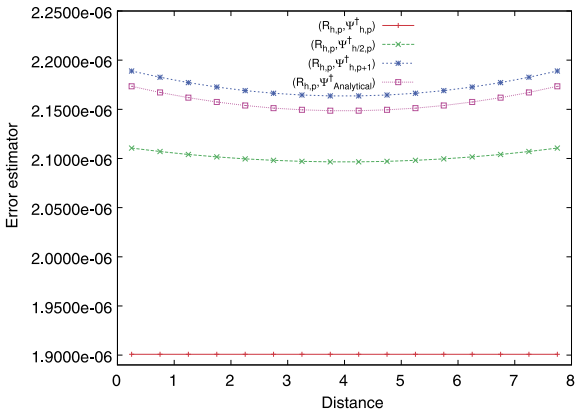

(b) Spatial variation of the error estimator with a uniform mesh of 16 cells

Fig. 4. Results for test case 1a. (For interpretation of the references to colour in this figure, the reader is referred to the web version of this article.)

6. Results and discussion

The results given by applying the test cases described in section 5 to the code are given and discussed in this section.

6.1. Test case 1a

The regularity of the solution and the fact that the goal is the integral value throughout the domain means that a uniform mesh is optimal for this problem. As a result, the AMR gives the same goal error convergence rate as uniform refinement (see Fig. 4a). The reason for this is due to the distribution of the DWR error indicator being fairly constant throughout the domain. The residual weighted by the analytical adjoint solution should give the same as the true goal error. This integral quantity was calculated and the cell-wise integral plotted (in blue) in Fig. 4b. This indicates a slightly larger contribution to the goal error from the edges of the domain, but not enough to justify non-uniform refinement. The distribution given by the approximate error indicators are also plotted in Fig. 4b. There is very little absolute difference between the three indicators, though it is clear that using a more accurate adjoint solution gives a more accurate error indicator distribution. For example, using a higher order mesh or a mesh with more cells for the adjoint solution results in the plot being slightly curved such as when the analytic solution is used, whereas using the same mesh as the forward equation gives a constant error indicator distribution. In this case using an adjoint of an increased order gives the distribution that is closest to the analytical distribution. This is most likely due to the regularity of the solution meaning that the accuracy of the solution is increased more by using a quadratic polynomial within the cells rather than increasing their number and using piece-wise linear polynomials.

6.2. Test case 1b

Due to the localised QoI, significant gains can be made through the use of AMR compared to uniform refinement (Fig. 5). However, in terms of mesh quality gained, there is no benefit to using more accurate error indicators (Fig. 5). Fig. 5 shows that the convergence rate of the AMR algorithm is much higher than uniform refinement for the first few mesh iterations before reaching an asymptotic convergence rate that is the same as the uniform refinement rate but at a lower absolute value of error per DoF. This is as expected, since there will be an optimum distribution of cells that will be achieved in the first few AMR meshes, beyond which the mesh will be refined uniformly to reduce the error in the QoI.

6.3. Test case 2a: Reed cell problem. Goal quantity: integral of the scalar flux throughout the whole domain

In the Reed cell problem we see from Fig. 6 that gains can be made by using goal-based refinement, even when the goal is the integral of the scalar flux throughout the whole domain. We also see that the convergence of the AMR is similar for all error indicators. This means that for this test case, using a more accurate approximation to the adjoint solution in the DWR compared to the forward solution does not result in a better mesh or improved goal error convergence. The convergence graph is slightly less stable for a starting mesh of 64 (Fig. 6a) compared to that of 320 (Fig. 6b). This is most likely due to the inaccuracies in the angular flux at low mesh resolutions for this test case. The non-negative flux criterion (see section 5) is met by half of the ordinates in the case of the 320 cell mesh, and not met for any of the ordinates when a 64 cell mesh is used. Thus, the inaccuracies in the flux and adjoint flux solution will be much bigger for the 64 cell mesh, meaning that the error indicators may give misleading information at the beginning of the AMR process.

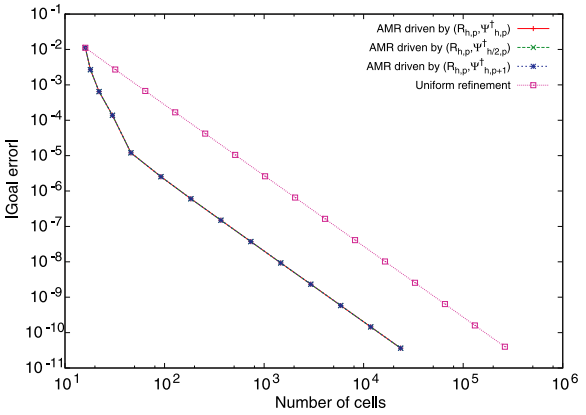

Fig. 5. Test case 1b: The absolute value of the goal error as a function of the cell number for uniform refinement and AMR driven by 3 different error indicators. AMR refinement criterion: refine if local error indicator $> 0.5 * maxerrorindicator$.

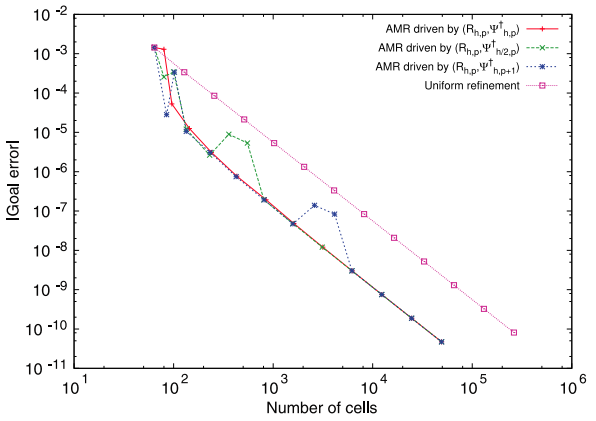

(a) Convergence with uniform starting mesh of 64 cells. Refinement criterion $= 0.3(maxerror)$

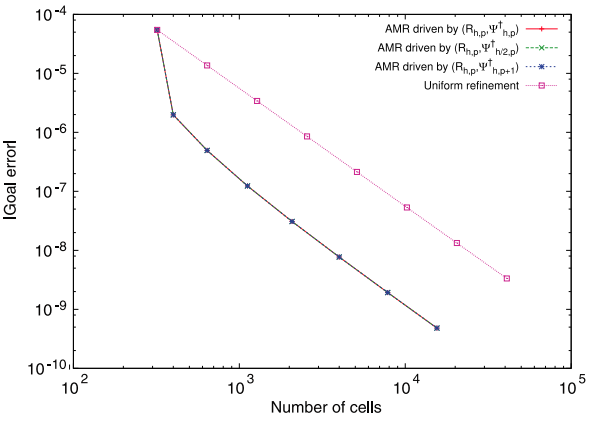

(b) Convergence with uniform starting mesh of 320 cells. Refinement criterion $= 0.3(maxerror)$

Fig. 6. Convergence results for test case 2a: Reed cell: goal being the integral of the scalar flux throughout the whole domain.

Fig. 7 shows the accuracy of the error estimators at various uniform refinement mesh iterations by plotting the *effectivity index* ($I_{h,p}$: the ratio of the magnitude of the error estimator to the magnitude of the true error in the QoI) against the number of cells. Fig. 7a shows that the error estimator using the adjoint solution of the same accuracy as the forward solution gives a very bad estimate of the error on the 64 cell mesh, by vastly over-estimating it. To better see how the accuracy of the error estimators vary with mesh refinement we remove this first point on the graph and re-plot in Fig. 7b. The error estimators consistently over-estimate the error and converge to a constant value of over-estimation. This is because the error estimators were calculated by summing the absolute value of the local error indicators. We have that:

$$|J(\psi) - J(\psi_h)| = \left| \sum_{i=1}^{nc} \sum_{j=1}^{m} (R_{h,j}, \psi_j^\dagger)_i \right| \leq \sum_{i=1}^{nc} \left| \sum_{j=1}^{m} (R_{h,j}, \psi_j^\dagger)_i \right| \tag{83}$$

Hence if $(R_h, \psi^\dagger_{approx.})_i$ is a good approximation to $(R_h, \psi^\dagger)_i$, an error estimator calculated in this way will tend to over-estimate the error unless the error has the same sign throughout the domain. This is desirable if we would like to be conservative in our stopping criteria, but may lead to the mesh being overly refined. If the absolute value is taken after summing the individual cell contributions, then we obtain the graph of Fig. 7c. Here we see that all of the DWR error estimators tested converge to the true error upon mesh refinement. It also shows that the best approximation is given by the more accurate solution calculated on the same mesh as the forward equation but using higher-order elements, it also consistently provides a conservative estimate in this example. The second best approximation is that given by the DWR using an adjoint calculated on a mesh that is twice as refined as the mesh used for the forward equation, using the first-order elements. Finally the worst estimate is given by using the adjoint solution calculated on the same cell number and order as the forward equation. Hence, although using an error indicator more accurate than $(R_h, \psi_{h,p})$ offers no benefit in terms of mesh refinement strategy, the resulting error estimator may not be sufficient for use as a stopping criteria in more complex

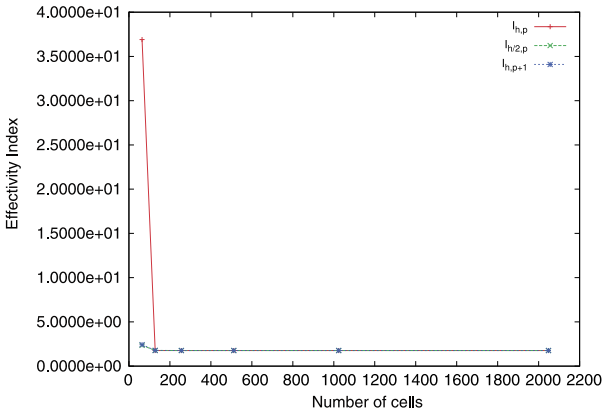

(a) $\frac{\sum_{i=1}^{nc} |\sum_{j=1}^{m} (R_{j,\mathrm{h}}, \psi^{\dagger}_{j,approx})_i|}{|truegoalerror|}$ for the first 6 meshes generated by uniform refinement from a uniform 64 cell starting mesh.

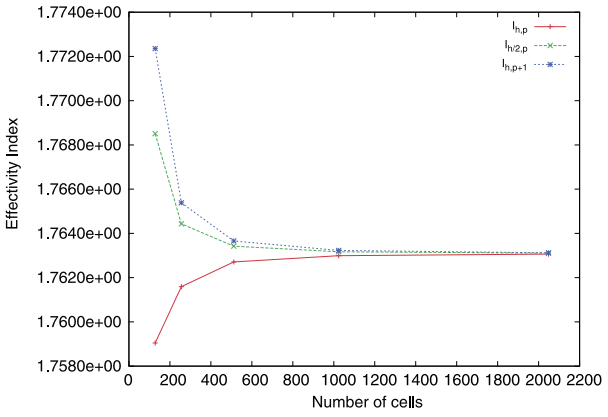

(b) $\frac{\sum_{i=1}^{nc} |\sum_{j=1}^{m} (R_{j,\mathrm{h}}, \psi^{\dagger}_{j,approx})_i|}{|truegoalerror|}$ for the first 5 meshes generated by uniform refinement from a uniform 128 cell starting mesh.

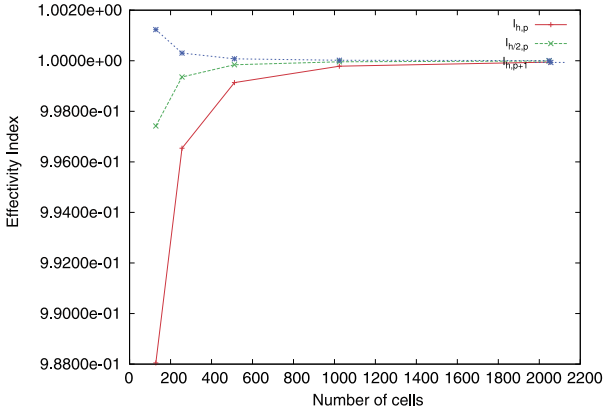

(c) $\left| \frac{\sum_{i=1}^{nc} \sum_{j=1}^{m} (R_{j,\mathrm{h}}, \psi^{\dagger}_{j,approx})_i}{truegoalerror} \right|$ for the first 5 meshes generated by uniform refinement from a uniform 128 cell starting mesh.

Fig. 7. Accuracy of the error in the QoI for test case 2a. Reed cell: goal being the integral of the scalar flux throughout the whole domain.

problems. One strategy that may achieve a compromise between these two methods would be to use the less accurate error indicators for mesh refinement until the goal error given by the resulting estimator was below the user-defined tolerance, and then verify that the solution is sufficiently accurate by calculating the more accurate error estimator at the end of the mesh refinement chain.

6.4. Test case 2b: Reed cell problem. Goal quantity: integral of the scalar flux throughout the first cm of the domain

Fig. 8a shows that AMR gives significant benefits in terms of number of unknowns needed for a given goal error accuracy compared to uniform refinement. We also note that in this case, using a better approximation for the adjoint solution in calculating the DWR results in an improved convergence rate.

Figs. 8b and 8c show that the DWR calculated using the same number of cells and the same order within each cell as that used for the forward equation overestimates the error in most cases. The first three points for $I_{h,p}$ in Fig. 8b show that the estimate over-estimates the true error by almost two orders of magnitude. The estimate then reduces significantly at the third mesh iteration (4th point on the plot). When the absolute value of the cell-wise values is not taken before summing over all cells, $I_{h,p}$ is reduced to 47.2 for the initial mesh, but the following three points in Fig. 8c remain the same as in Fig. 8b. Fig. 8d shows only the ratio of the DWR estimate of the goal error and the analytically computed value for the case where the adjoint is computed on a mesh twice as refined, and the case where it is computed on a mesh using everywhere higher-order elements. Here we see that the result is much better estimated, particularly by the higher-order approximation, until the 4th mesh iteration. At this point, both estimators significantly under-estimate the error.

The comments made above on Fig. 8 can be explained by Fig. 9. In the zeroth mesh (Fig. 9a) it is clear that in the problem regions, i.e. the first cm where the goal region is, and the second cm where there is a high value of error, the

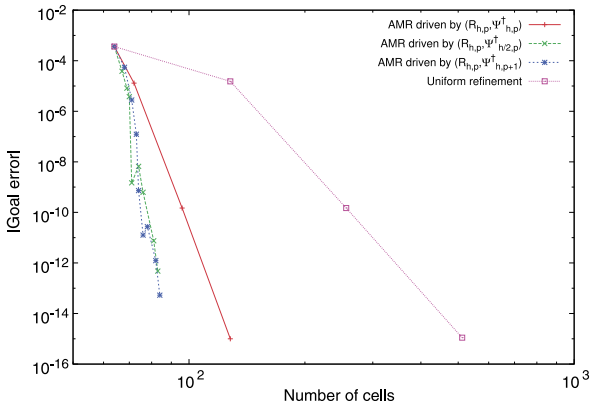

(a) Convergence with uniform starting mesh of 64 cells. Refinement criterion = $0.3(maxerror)$

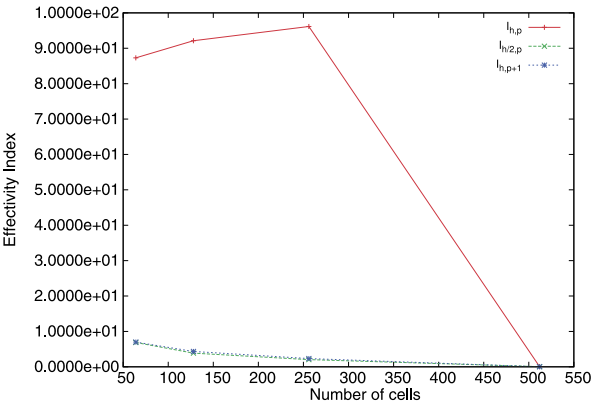

(b) $\frac{\sum_{i=1}^{nc}|\sum_{j=1}^{m}(R_{j,\mathrm{h}},\psi^{\dagger}_{j,approx})_i|}{|truegoalerror|}$ for the first 4 meshes generated by uniform refinement from a uniform 64 cell starting mesh.

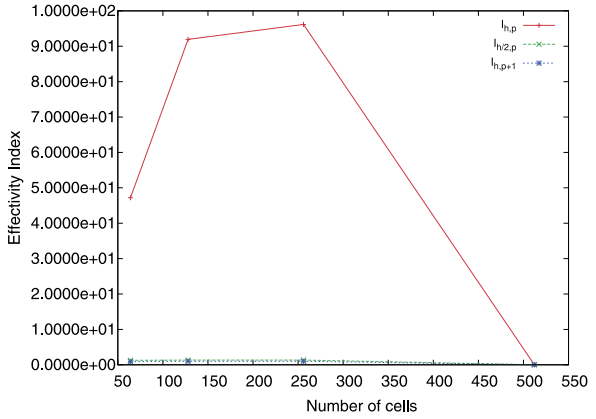

(c) $\left|\frac{\sum_{i=1}^{nc}\sum_{j=1}^{m}(R_{j,\mathrm{h}},\psi^{\dagger}_{j,approx})_i}{truegoalerror}\right|$ for the first 4 meshes generated by uniform refinement from a uniform 64 cell starting mesh.

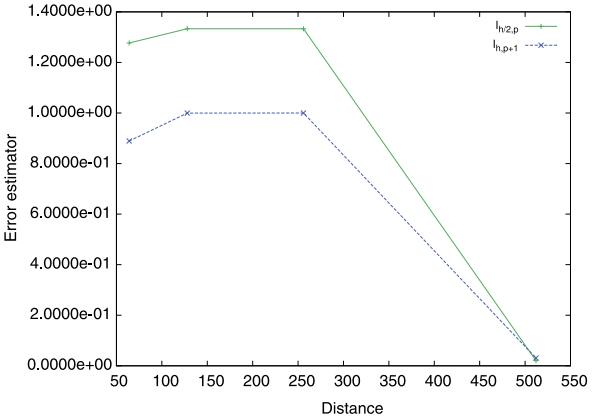

(d) $\left|\frac{\sum_{i=1}^{nc}\sum_{j=1}^{m}(R_{j,\mathrm{h}},\psi^{\dagger}_{j,approx})_i}{truegoalerror}\right|$ for the first 4 meshes generated by uniform refinement from a uniform 64 cell starting mesh.

Fig. 8. Results for test case 2b: Reed cell: goal being the integral of the scalar flux throughout the first 1 cm of the domain. Uniform refinement starting from 64 cells.

less accurate error estimator drastically over-estimates the error. This is most likely due to the fact that the DD solution oscillates in regions of high total cross sections and mesh cell sizes that are not small enough.

The fact that the error estimator deteriorates significantly by mesh iteration 3 (see Fig. 8d) is explained by the fact that at this point, all local error indicators have a value below that which can be reliably represented by double floating point precision (see Fig. 9d), so the results cannot be trusted.

6.5. Test case 3a: EIRA-1-D problem. Goal quantity: integral of the scalar flux throughout the whole domain

Fig. 10a shows the gains obtained in terms of the convergence of the goal error when using AMR, even when this goal is the integral of the scalar flux throughout the domain. Due to the presence of less extreme gradients in this solution compared to the Reed cell problem, the gains due to AMR are less compared to those shown in Fig. 6. The convergence behaviour was also found to be similar for different starting meshes, and that using a more accurate error indicator does not result in a better convergence rate.

Fig. 10b shows that if the absolute value of the local error indicator is taken before summing over all cells, then the DWR estimator converges to an over-estimation of the true error in the QoI. Fig. 10c shows that when the absolute value is taken after summing over all cells, a more accurate approximation of the adjoint solution results in a more accurate DWR estimate. Though the difference in accuracy is small.

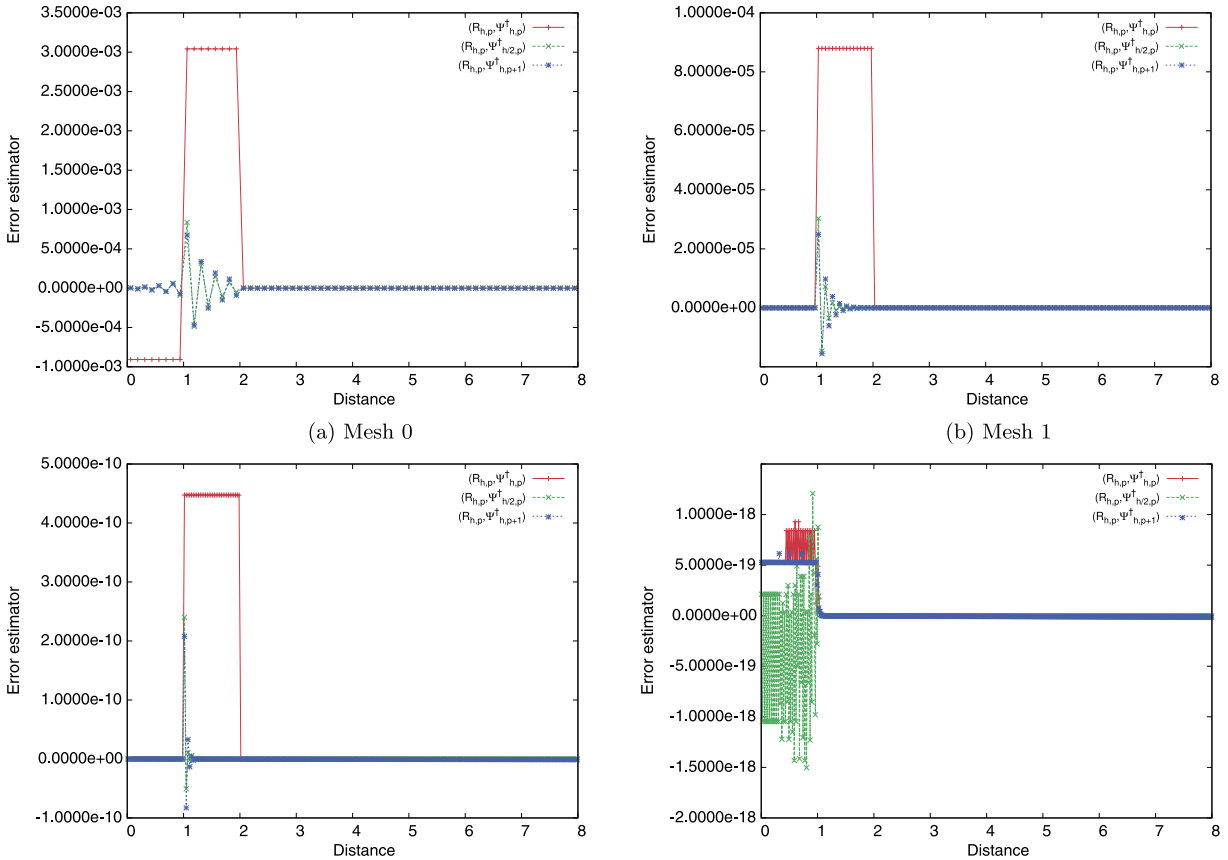

(a) Mesh 0 (b) Mesh 1

(c) Mesh 2 (d) Mesh 3

Fig. 9. The spatial variation of the error indicators, $(R_h, \psi^{\dagger}_{approx})_{cell}$, as uniform refinement is performed for test case 2b with a 64 cell starting mesh: Reed cell: goal being the integral of the scalar flux throughout the first 1 cm of the domain.

6.6. Test case 3b: EIRA-1-D problem. Goal quantity: integral of the scalar flux throughout the first cm of the domain

Fig. 11a shows that a reduction of the number of cells required to give an accurate solution to the QoI is achieved through goal-based AMR. This improvement is slightly more than that seen in Fig. 10a because the QoI is more localised. This is generally true for test cases where the residual distribution does not vary very much throughout the domain. This is because the severity of the spatial variation of the DWR is then highly dependent on the adjoint solution, which depends on the localisation of the adjoint source, which is determined by the QoI.

In this test case, summing the absolute values of all the error indicators for each cell over-estimates the error no matter which approximation to the adjoint solution is used (Fig. 11b). Fig. 11c shows that all error estimates converge to the analytical error if the absolute values of the local indicators are not taken before summing over all cells. In this case we see that the error estimates using adjoint solutions of higher accuracy both consistently over-estimate the error, whereas using an adjoint solution computed with the same number of mesh cells and the same within-cell polynomial representation as the forward equation under-estimates the error. The effectivity indices as plotted in Fig. 11c show that the best approximation to the error, for this test case, is given by the one using an adjoint solution calculated on a mesh everywhere twice as refined as the forward solution. The effectivity index resulting from using everywhere higher order cells for the adjoint solution deviates from one slightly more than the case where an adjoint solution is calculated on the same mesh as the forward equation, but has the advantage of not under-estimating the error.

6.7. Test case 4: K_{eff} goal quantity

Fig. 12a shows that AMR gives the same convergence rate as uniform refinement. This shows that uniform refinement is optimal for this test case. This is due to the problem being homogeneous, with fissionable material throughout. The uniform distribution of fissionable material results in everywhere in the domain being important for the goal quantity. The smoothness of the solution results in very little variation of the overall error (due to both flux directions combined). Thus uniform refinement is optimal for this test case.

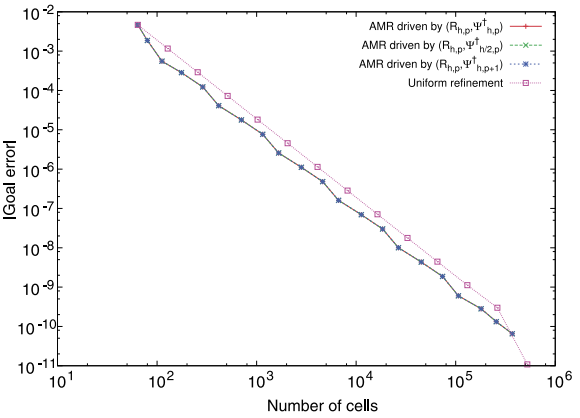

(a) Convergence with uniform starting mesh of 64 cells. Refinement criterion = $0.3(maxerror)$

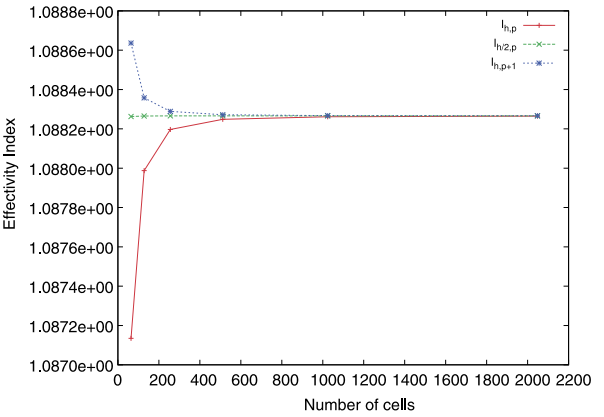

(b) $\frac{\sum_{i=1}^{nc} |\sum_{j=1}^{m}(R_{j,\mathrm{h}},\psi^{\dagger}_{j,approx})_i|}{|truegoalerror|}$ for the first 6 meshes generated by uniform refinement from a uniform 64 cell starting mesh.

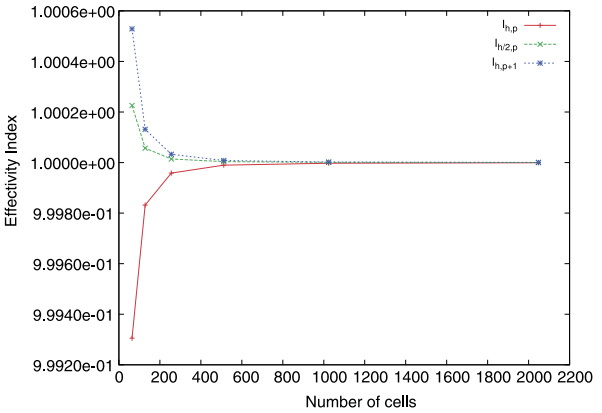

(c) $\left|\frac{\sum_{i=1}^{nc}\sum_{j=1}^{m}(R_{j,\mathrm{h}},\psi^{\dagger}_{j,approx})_i}{truegoalerror}\right|$ for the first 6 meshes generated by uniform refinement from a uniform 64 cell starting mesh.

Fig. 10. Results for test case 3a: EIRA-1-D problem: goal being the integral of the scalar flux throughout the whole domain.

Fig. 12b shows the accuracy of the error estimators. All error estimates tend to an effectivity index of one as the mesh is refined. Despite giving the worst result for the effectivity index at low mesh refinements, the estimator using the same mesh for both forward and adjoint solutions converges rapidly to unity as the mesh is refined and has an error of only 4.1% for the initial mesh. Improvements are observed when a more accurate solution to the adjoint equation is used. Out of the two options tested here, the error estimate using the adjoint solution calculated using everywhere higher order cells gives the best approximation to the true goal error. It is due to the smoothness of the analytical solution that increasing the within-cell order of the adjoint solution gives a better approximation than by doubling the number of cells in the mesh.

7. Conclusions and further work

This work has described the development and application of DWR type error estimation for the standard and higher-order DD-S_N discretisation of the neutron transport equation in 1-D. The WR view of the DD scheme in 1-D allows for a functional representation of the flux approximation that exists in a subspace of H^1. Thus, a residual can be computed from the approximate solution and weighted by a solution to an approximate adjoint equation computed in the same manner. It was also shown that the DD solution to the adjoint equation must be found by discretising the adjoint equation directly and not by transposing the discretised forward operator since the method is not adjoint consistent. Computationally, the implementation of this is not difficult due to the sweep algorithm employed in the DD scheme.

The DWR calculated over a cell provided local error indicators for the DD-S_N AMR procedure. This was applied to both fixed source and eigenvalue (K_{eff} criticality) problems. A reduction in the number of DoF was observed for heterogeneous problems and homogeneous problems that had localised QoI. Therefore, this work has demonstrated that a reduction in the

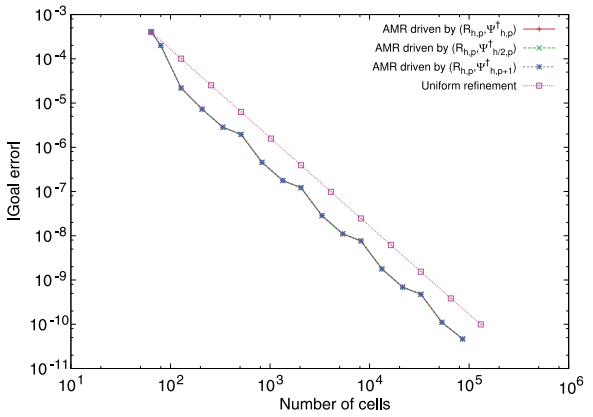

(a) Convergence with uniform starting mesh of 64 cells. Refinement criterion = $0.3(maxerror)$

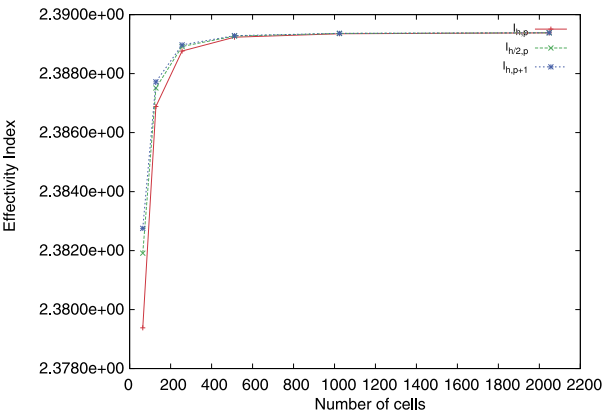

(b) $\frac{\sum_{i=1}^{nc} |\sum_{j=1}^{m}(R_{j,h},\psi^{\dagger}_{j,approx})_i|}{|truegoalerror|}$ for the first 6 meshes generated by uniform refinement from a uniform 64 cell starting mesh.

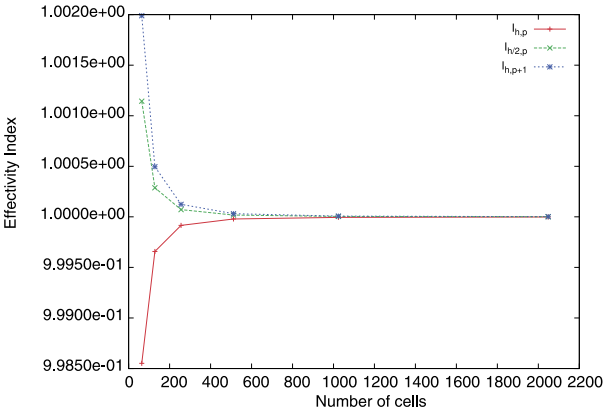

(c) $\left|\frac{\sum_{i=1}^{nc}\sum_{j=1}^{m}(R_{j,h},\psi^{\dagger}_{j,approx})_i}{truegoalerror}\right|$ for the first 6 meshes generated by uniform refinement from a uniform 64 cell starting mesh.

Fig. 11. Results for test case 3b: EIRA-1-D problem: goal being the integral of the scalar flux throughout the first cm of the domain.

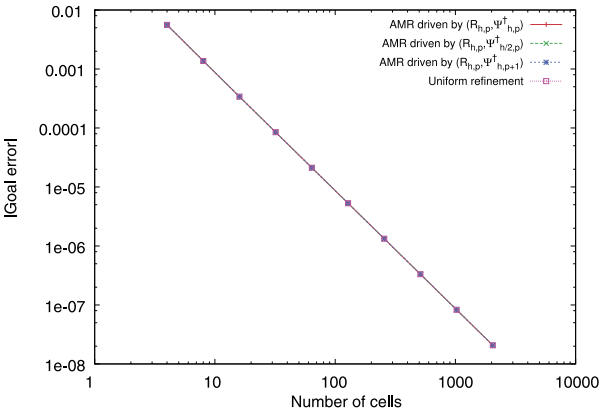

(a) The true goal error as a function of cell numbers generated by uniform refinement.

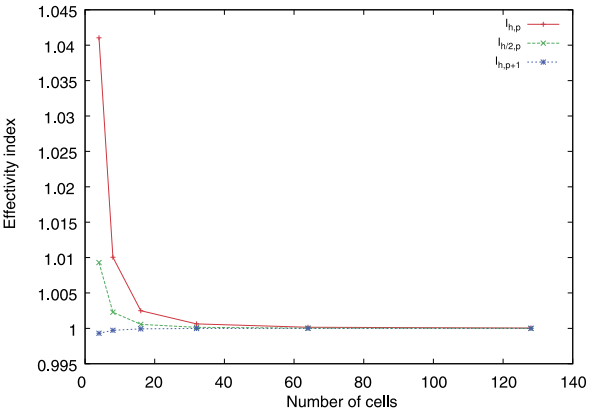

(b) $\left|\frac{\sum_{i=1}^{nc}\sum_{j=1}^{m}(R_{j,h},\psi^{\dagger}_{j,approx})_i}{truegoalerror}\right|$ for the first 6 meshes generated by uniform refinement from a uniform 4 cell starting mesh.

Fig. 12. Test case 4: results where the goal is the K_{eff}.

number of unknowns required to reach an accurate solution to a QoI defined by a functional of the angular flux can be achieved in some cases with the use of DWR driven AMR.

Using the same mesh cell number and order as the forward solution for the adjoint solution gave a good approximation to the true error in the QoI for most cases. The only time it was not sufficiently accurate was for low order meshes in test case 2a, and for all meshes in test case 2b. In more challenging test cases, it may be useful to use a more accurate mesh representation for the adjoint solution if the DWR estimator is to be used as a stopping criteria. In test cases with large discontinuities, or where there are regions not satisfying the negative flux criterion, a better estimator is given by the E_2 estimator than E_3.

In general, it was found that using a higher-order approximation to the adjoint solution for the DWR error indicators did not result in the AMR giving a better convergence graph. The exception was where the goal was in a region heavily affected by the instability of the DD-S_N solution, in areas with large total cross sections. Sometimes there is sensitivity to the initial mesh chosen, especially if the cell sizes do not satisfy the negative flux criterion.

A good compromise suggested was to use the least accurate error indicators for mesh refinement until that gives a goal error below a user-defined tolerance, and then use the more accurate error estimator to verify this convergence.

The DWR error estimate for the goal functional is obtained by summing the values calculated locally for each cell (the error indicators). The absolute values of the indicators are compared for mesh refinement. It was shown that if the absolute values of the indicators are summed over all cells to obtain an error estimate for the functional, the effectivity index will tend to a value that is ≥ 1 as the mesh is uniformly refined. Using this as an error estimator has the advantage of being conservative, but can lead to over-refinement. When the absolute value was not taken before summing over the indicators the effectivity index tended to 1 for all test cases apart from when the limits of double precision floating point accuracy were reached (such as in test case 2b).

Given that using Hennart's formulation for the diamond difference technique allows us to specify higher-order solutions within a cell, p and hp refinement such as was implemented by other researchers in the transport community would be possible here. This could potentially be a promising area for future research.

Use of DWR estimators for iterative solver stopping criteria such as in [30,31] could also be investigated in further work.

Extending these DWR (goal-based) error estimators to multiple spatial dimension applications would also be desirable, so that more complex problems in reactor physics and radiation shielding can be analysed.

Acknowledgements

R.S. Jeffers would like to thank EPSRC for their support through the EPSRC grant "Industrial Doctorate Centre: Nuclear Engineering" (EPSRC grant number: EP/G037426/1) as well as EDF R&D for their industrial support. Dr M.D. Eaton and Dr J. Kophazi would like to thank EPSRC for their support through the following grants: "Adaptive Hierarchical Radiation Transport Methods to Meet Future Challenges in Reactor Physics" (EPSRC grant number: EP/J002011/1) and "RADIANT: A Parallel, Scalable, High Performance Radiation Transport Modelling and Simulation Framework for Reactor Physics, Nuclear Criticality Safety Assessment and Radiation Shielding Analyses" (EPSRC grant number: EP/K503733/1).

The authors would also like to thank Dr James S. Warsa for his quick response and help with queries involving the Maple command scripts written for computing analytical solutions to the 1-D S_N equations.

In accordance with EPSRC funding requirements, the supporting data used to create the figures in this article may be accessed at the following DOI: https://doi.org/10.5281/zenodo.258377.

References

[1] NEA, PARTISN 4.00: 1-D, 2-D, 3-D time-dependent, multigroup deterministic parallel neutral particle transport code, Web, http://www.oecd-nea.org/tools/abstract/detail/ccc-0707, 2009, CCC-0707 PARTISN 4.00.

[2] Thomas M. Evans, Alissa S. Stafford, Rachel N. Slaybaugh, Kevin T. Clarno, Denovo: a new three-dimensional parallel discrete ordinates code in scale, Nucl. Technol. 171 (August 2010) 171–200.

[3] Salli Moustafa, Ivan Dutka-Malen, Laurent Plagne, Angélique Ponçot, Pierre Ramet, Shared memory parallelism for 3D Cartesian discrete ordinates solver, in: Joint International Conference on Supercomputing in Nuclear Applications and Monte Carlo 2013, SNA + MC 2013. Pluri- and Trans-Disciplinarity, Towards New Modeling and Numerical Simulation Paradigms, Ann. Nucl. Energy (ISSN 0306-4549) 82 (2015) 179–187, http://dx.doi.org/10.1016/j.anucene.2014.08.034, http://www.sciencedirect.com/science/article/pii/S0306454914004265.

[4] Yaqi Wang, Jean C. Ragusa, Standard and goal-oriented adaptive mesh refinement applied to radiation transport on 2-D unstructured triangular meshes, J. Comput. Phys. (ISSN 0021-9991) 230 (3) (2011) 763–788, http://dx.doi.org/10.1016/j.jcp.2010.10.018, http://www.sciencedirect.com/science/article/pii/S0021999110005747.

[5] Bruno Turcksin, Jean C. Ragusa, Wolfgang Bangerth, Goal-oriented h-adaptivity for the multigroup SP_N equations, Nucl. Sci. Eng. 165 (2010) 305–319.

[6] Mark Ainsworth, J. Tinsley Oden, A posteriori error estimation in finite element analysis, Comput. Methods Appl. Mech. Eng. (ISSN 0045-7825) 142 (1–2) (1997) 1–88, http://dx.doi.org/10.1016/S0045-7825(96)01107-3, http://www.sciencedirect.com/science/article/pii/S0045782596011073.

[7] Yaqi Wang, Jean Ragusa, Application of hp adaptivity to the multigroup diffusion equations, Nucl. Sci. Eng. 161 (2009) 22–48.

[8] Wolfgang Bangerth, Rolf Rannacher, Adaptive Finite Element Methods for Differential Equations, Lectures in Mathematics. ETH Zürich, Birkhäuser Verlag, 2003.

[9] D. Lathouwers, Goal-oriented spatial adaptivity for the S_N equations on unstructured triangular meshes, Ann. Nucl. Energy (ISSN 0306-4549) 38 (6) (2011) 1373–1381, http://dx.doi.org/10.1016/j.anucene.2011.01.038, http://www.sciencedirect.com/science/article/pii/S0306454911000594.

[10] D. Lathouwers, Spatially adaptive eigenvalue estimation for the S_N equations on unstructured triangular meshes, Ann. Nucl. Energy (ISSN 0306-4549) 38 (9) (2011) 1867–1876, http://dx.doi.org/10.1016/j.anucene.2011.05.013, http://www.sciencedirect.com/science/article/pii/S0306454911002039.

[11] Mark A. Goffin, Christopher M.J. Baker, Andrew G. Buchan, Christopher C. Pain, Matthew D. Eaton, Paul N. Smith, Minimising the error in eigenvalue calculations involving the Boltzmann transport equation using goal-based adaptivity on unstructured meshes, J. Comput. Phys. 242 (2013) 726–752.
[12] Mark A. Goffin, Andrew G. Buchana, Anca C. Belme, Christopher C. Pain, Matthew D. Eaton, Paul N. Smith, Richard P. Smedley-Stevenson, Goal-based angular adaptivity applied to the spherical harmonics discretisation of the neutral particle transport equation, Ann. Nucl. Energy 71 (2014) 60–80.
[13] Jose I. Duo, Yousry Y. Azmy, Ludmil T. Zikatanov, A posteriori error estimator and AMR for discrete ordinates nodal transport methods, in: PHYSOR 2008, Ann. Nucl. Energy (ISSN 0306-4549) 36 (3) (2009) 268–273, http://dx.doi.org/10.1016/j.anucene.2008.12.008, http://www.sciencedirect.com/science/article/pii/S0306454908003368.
[14] HyeongKae Park, Cassiano R.E. de Oliveira, Coupled space-angle adaptivity for radiation transport calculations, Nucl. Sci. Eng. 161 (2009) 216–234.
[15] Krzysztof J. Fidkowski, David L. Darmofal, Review of output-based error estimation and mesh adaptation in computational fluid dynamics, AIAA J. 49 (4) (2011) 673–694.
[16] Niles A. Pierce, Michael B. Giles, Adjoint recovery of superconvergent functionals from PDE approximations, SIAM Rev. 42 (2) (2000) 247–264.
[17] M.B. Giles, N.A. Pierce, E. Süli, Progress in adjoint error correction for integral functionals, Comput. Vis. Sci. 6 (2004) 113–121.
[18] Qingshan Chen, Max Gunzburger, Goal-oriented a posteriori error estimation for finite volume methods, J. Comput. Appl. Math. 265 (2014) 69–82.
[19] David A. Venditti, David L. Darmofal, Grid adaptation for functional outputs: application to two-dimensional inviscid flows, J. Comput. Phys. 176 (2002) 40–69.
[20] Dmitri Kuzmin, Sergey Korotov, Goal-oriented a posteriori error estimates for transport problems, Math. Comput. Simul. 80 (2010) 1674–1683.
[21] Dmitri Kuzmin, Matthias Möller, Goal-oriented mesh adaptation for flux-limited approximations to steady hyperbolic problems, J. Comput. Appl. Math. 233 (2010) 3113–3120.
[22] J.B. Collins, D. Estep, S. Tavener, A posteriori error estimation for the Lax–Wendroff finite difference schemes, J. Comput. Appl. Math. (ISSN 0377-0427) 263 (0) (2014) 299–311, http://dx.doi.org/10.1016/j.cam.2013.12.035, http://www.sciencedirect.com/science/article/pii/S0377042713007085.
[23] J.P. Hennart, E. del Valle, A generalized nodal finite element formalism for discrete ordinates equations in slab geometry: Part I: Theory in the continuous moment case, Transp. Theory Stat. Phys. 24 (1995) 449–478.
[24] Roland Becker, Rolf Rannacher, An optimal control approach to a posteriori error estimation in finite element methods, Acta Numer. 10 (2001) 1–102.
[25] Juhani Pitkäranta, On the spatial differencing of the discrete ordinate neutron transport equation, SIAM J. Numer. Anal. 15 (1978) 859–869.
[26] J.T. Oden, J.N. Reddy, An Introduction to the Mathematical Theory of Finite Elements, John Wiley and Sons, 1976.
[27] J.N. Reddy, Applied Functional Analysis and Variational Methods in Engineering, McGraw–Hill, 1986.
[28] R.S. Jeffers, Spatial Goal-Based Error Estimation and Adaptive Mesh Refinement (AMR) for Diamond Difference Discrete Ordinate (DD-S_N) Methods, EngD thesis, Imperial College London, 2017.
[29] George I. Bell, Samuel Glasstone, Nuclear Reactor Theory, Van Nostrand Reinhold Company, 1970.
[30] D. Meidner, R. Rannacher, J. Vihharev, Goal-oriented error control of the iterative solution of finite element equations, J. Numer. Math. 17 (2009) 143–172.
[31] R. Rannacher, A. Westenberger, W. Wollner, Adaptive finite element solution of eigenvalue problems: balancing of discretization and iteration error, J. Numer. Math. 18 (2010) 303–327.
[32] William H. Reed, New difference schemes for the neutron transport equation, Nucl. Sci. Eng. 36 (1971) 309–314.
[33] James.S. Warsa, Analytical S_N solutions in heterogeneous slabs using symbolic algebra computer programs, Ann. Nucl. Energy 29 (2002) 851–874.
[34] E.E. Lewis, W.F. Miller Jr., Computational Methods of Neutron Transport, American Nuclear Society Inc., 1993.
[35] J. Stepanek, T. Auerbach, W. Halg, Calculation of Four Thermal Reactor Benchmark Problems in x-y Geometry, Technical Report 464, Federal Institute of Technology, Zurich, 1982.
[36] C.E. Siewert, The critical problem with high-order anisotropic scattering, Ann. Nucl. Energy 28 (2001) 825–829.